Dear Matthew Hecht,

please find below our point by point response to all referee comments. We would like to thank the referees for their helpful suggestions. We also fixed a few additional language/ grammar issues that were identified through our repeated proof-reading. The difference file and revised manuscripts are appended below.

———————————————————————————————————

Anonymous Referee #1

GENERAL COMMENTS

I summarize this paper as follows:

Turbulent transport estimates may be inferred from observations of the large-scale hydrography, but may not be useful or meaningful because they often neglect crucial physics. Using inverse methods on GCMS and complimentary datasets can help, but the method itself remains unevaluated. This paper uses a state estimate inversion, augmented by the inclusion of Argo profiles, to estimate turbulent transport rates. It also addresses questions about the precision and generality of such an inversion. A key finding is that the inferred diffusivities (GM, iso- and diapycnal) strongly improve the ocean stratification of the state estimate in relation to the in situ Argo profiles. The stratification in the upper ocean is shown to be highly sensitive to changes in the eddy transport coefficients. The new coefficients significantly improve model bias of passive, biogeochemical tracers. The state estimate is compared to similar, earlier estimates to gauge the robustness of the results, without providing a formal error estimate (which would be intractable).

This work satisfies all requirements of a publishable manuscript as listed on the OSD peer review guide (http://www.ocean-science.net/peer_review/review_criteria.html). The paper as a whole is well written, and the authors provide a nice set of comparisons between new and old state estimates (and in situ data) to show where the Argo data improves things. The paper is straightforward to read and the figures are organized in a way that supports the main arguments well. Aside from a few points (see below) where I feel the authors could have refined their choice of words, I find this paper to be of high scientific and educational value. It does provide a significant improvement over previous work on the same theme, and for the most part justifies why the Argo profiles provide this improvement while remaining cautious about the overall limitations of the method.
We thank the referee for expressing such strong support for this study.

SPECIFIC COMMENTS

On pg. 1113, line 26, the authors claim that the large adjustments in the top 2000 m may be due to the inclusion of the Argo observations. I think this claim would be stronger if there was an additional figure showing the same plots from an inversion without Argo. Would the magnitude of the adjustments decrease substantially?

Thanks for pointing this out. This statement was just meant, at this point, to announce the central subject of sections 3 and 4, which is now done more clearly. Furthermore, questioning the relative importance of what Argo brings compared with earlier constraints is valid. In response to this, we now provide an additional diagnostic (new Fig. 5, discussed at the start of section 3). It compares adjoint sensitivities for altimetry and Argo data. The results show that the constraint on turbulent transport parameters provided by one decade of Argo data is stronger than that provided by even two decades of altimetry. An extensive and systematic exploration of this topic would go beyond the scope of this paper and would require re-doing the full ocean state estimate without the Argo data (as suggested by the referee and our concluding section). Our statement of this perspective (next to last paragraph of the paper) was made more obvious.

Pg. 1115, line 10: This statement is too strong, or perhaps "constrained" is not the right word here. The Argo profiles themselves are not constraining the oxygen minimum, though they do constrain the inversion for the diffusivities that affect the minimum (either directly through improved eddy transport rates, or indirectly through improvement of other physical variables that impact biogeochemistry).
Thanks for pointing this out. The statement on Pg. 1115, line 10 was indeed unclear and should be understood in the light of the statement on L17-20 p 1114. The two statements have been brought together at the end of section 2 to clarify this point. Also "strong evidence" was replaced with just "evidence".

Pg. 1116, line 6: Another strongly worded statement. I'd change "is largely due" to "is noticeably improved by the use of".
Done.

TECHNICAL CORRECTIONS

Pg. 1111, line 29: "reduces" should be "reduce".
Fixed.

Pg. 1112, line 20: remove "and"
Sentence was revised so that it becomes more clear why "and" is in fact needed.

Figure 1: I see that the same figure appears in Forget et al. (2015), but I think it could use more information in the caption here. Does the color scale refer to percentage differences?
Missing product names were added in the figure. Methodological differences were added in the caption. The color scale unit statement (degree C) was clarified. Please note that the Forget et al. (2015) plot is analogous but shows salinity misfits instead of temperature misfits.

Pg. 1113, line 21: "energetic" should be "energetics"
Fixed.

Pg. 1114, line 4: should be "two model integrations are carried out for 500 years"
Fixed.

Pg. 1115, line 3: "parameters" should be "parameter"
Fixed.

Pg. 1115, line 6: "maintaining" should be "maintenance"
Fixed.

Pg. 1118, line 14: “defended observability proposition" is kind of strange wording and is vague. I think adding a sentence reviewing the "observability proposition" and stating it very clearly would help here.
We replaced “defended observability proposition” with an explicit statement. The other instance of this phrase (at L20 p1116 in the original submission) was also removed.

Pg. 1122, line 17: "coast of Antarctica"
Fixed.

Pg. 1126, line 5: "variety of numerical models”
Fixed.

———————————————————————————————————

Anonymous Referee #2

This study shows that observations of the large scale stratification by Argo yield useful constraints to estimate turbulent transport parameters in the ocean.While the parameter estimation significantly reduces the misfits wrt to temperature and salinity as well as non-assimilated biogeochemical tracers, …

it seems questionable if the parameters are entirely physically reasonable or if they reflect other model errors. My main concern is the physicality of the mixing parameters, …
Errors in data interpretation is always a valid concern, and we are certainly cautious in stressing that the results are necessarily imperfect in the paper. In contrast with e.g. the Whalen and Cole studies that do not question the validity of the conceptual models being used to interpret Argo data, this paper includes extensive discussion of uncertainties and caveats (in sections 1, 5 and 6).

General circulation model errors unrelated to turbulent transport parameters remain, admittedly, poorly understood. In fact, to the best of our knowledge, Forget et al 2015 is the first attempt at quantifying the relative importance of structural versus parametric model errors in GCMs. Relevant results are now recalled in sections 5 and 6.

and a better discussion/comparison to the differences in approach and results of Liu et al. What distinguishes this study from Liu, Koehl and Stammer? It seems the focus here is more on the Argo data, but Liu et al. also used the Argo data as constraints.
The presentation of this comparison (section 5) indeed needed to be clarified and complemented. Firstly, Kredi and Kz were added in Fig10 (now Fig11) to better reveal differences between the ECCO v4 and Liu et al results. Secondly, the opening paragraph of section 5 was expanded into three separate paragraphs to highlight some of the ECCO v4 innovations and differences as compared with Liu et al.

The doubled duration of ECCO v4 is a huge factor as shown by the new Fig. 5 (first discussed in section 3). It is unclear what data Liu et al refer to as "Argo" given that the actual Argo array deployment had barely started by 2001 and its full deployment was only reached by 2005. As documented in the new Fig. 5 caption, more than 98% of Argo profiles were obtained after 2001 (i.e. excluded from the Liu et al experiment).

The primary objective of this paper (revealing Argo's constraints) is we believe clearly stated (starting with the paper's title) and quite different from Liu et al's. Besides, the presented analyses of, e.g, stratification (Figs 6&7), mixed layer depths (Figs 6&8), multi-centennial model drifts (Figs 3&4), and biogeochemistry (Figs 3&4) are all original — these important aspects of ocean state estimation are not covered by Liu et al.

please specify what are your control parameters exactly?
Added missing uncertainty specifications for internal parameter controls. The frequency of atmospheric controls was further repeated from Forget et al 2015.

Figure 1: if you show all of those panels I think you should also describe in more detail how the experiments differed and not only refer to another paper.
Missing product names were added in the figure. Methodological differences were added in the caption. The solutions are only discussed in groups in this paper: (1) ECCO v4 vs (2) other 1° ECCO estimates and (3) ECCO2 eddying solutions at 1/6° resolution. The grouping corresponds to different representation of turbulent transports, as stated in the caption. The grouping was highlighted in the figure to make this immediately clear.

The authors should compare their Redi diffusivity estimates to recent Argo data based eddy diffusion estimates by S. Cole et al. "Eddy stirring and horizontal diffusivity from Argo float observations: Geographic and depth variability". GRL, 2015.
Thanks for pointing out this very recent paper that we had not noticed yet. References to Cole et al 2015 were added in section 1 (paragraph 1) and section 4 (paragraph 6).

section 4, GM and Redi coefficients: What do you mean by "can be defended on theoretical grounds" (Marshall, 2006). What theory are you refering to? I think Marshall (2006) would be refering to the Redi rather than the GM coefficient. Do you see any evidence of a steering level effect (enhanced mixing where the Rossby wave speed equals the mean flow speed) in the Redi coefficient?
The statement in section 4 regarding Kgm was indeed confusing. Please note that Marshall et.al (2006) do not refer clearly to Kgm or Kredi because their surface eddy diffusivities do not unambiguously map onto either one (for reasons explained in e.g. Ferreira and Marshall, 2006). We have therefore removed the statement and instead point to the discussion of comparable results in the Ferreira et al and Liu et al inversions. Regarding steering level effects in Kredi (where there is a an available theoretical background), there are hints of it in the extended Fig11 that interestingly were not seen in Liu et al's result. This point was added in section 5.

It is striking that the GM coefficient (Figure 8 top) has minima in the Western Boundary Currents (see also section 6, line 15, can you comment on the differences). Do you allow for a negative GM coefficient to occur?
We do not allow negative GM coefficients (as stated in section 2). The reviewer's point regarding Kgm minima in Fig 8 is now better reflected in section 5 (when discussing Kgm

in the Gulf Stream) and section 6 (when discussing mid-latitude jets more generally). Please note that Liu et al also found Kgm minima in western boundary currents.

section 4, diapycnal diffusivity: can you comment on the apparent "missing mixing" in the ACC? As compared to Whalen et al. it seems one striking difference is in the Southern Ocean. Is there any evidence for links to topography?
The point on Kd in the ACC was added in the uncertainty section. There is weak evidence of links to topography in Kd near the sea floor, as was already noted (also in section 5). In the upper ocean things are less clear, and should be addressed in further studies.

Manuscript prepared for Ocean Sci. Discuss.
with version 2014/09/16 7.15 Copernicus papers of the LaTeX class copernicus.cls.
Date: 19 September 2015

On the observability of turbulent transport rates by Argo: supporting evidence from an inversion experiment

G. Forget[1], D. Ferreira[2], and X. Liang[1]

[1]Dept. of Earth, Atmospheric and Planetary Sciences, Massachusetts Institute of Technology, Cambridge, MA 02139, USA
[2]Department of Meteorology, University of Reading, Reading, UK

Correspondence to: G. Forget (gforget@mit.edu)

Discussion Paper | Discussion Paper | Discussion Paper | Discussion Paper |

Abstract

Although estimation of turbulent transport parameters using inverse methods is not new, there is little evaluation of the method in the literature. Here, it is shown that extended observation of the ~~broad scale~~ broad-scale hydrography by Argo provides a path to improved estimates of regional turbulent transport rates. Results from a 20 year ocean state estimate produced with the ECCO v4 non-linear inverse modeling framework provide supporting evidence. Turbulent transport parameter maps are estimated under the constraints of fitting the extensive collection of Argo profiles collected through 2011. The adjusted parameters dramatically reduce misfits to in situ profiles as compared with earlier ECCO solutions. They also yield a clear reduction in the model drift away from observations over multi-century long simulations, both for assimilated variables (temperature and salinity) and independent variables (~~bio-geochemical~~ biogeochemical tracers). Despite the minimal constraints imposed specifically on the estimated parameters, their geography is physically plausible and exhibits close connections with the upper ocean ocean stratification as observed by Argo. The estimated parameter adjustments furthermore have first order impacts on upper-ocean stratification and mixed layer depths over 20 years. These results identify the constraint of fitting Argo profiles as an effective observational basis for regional turbulent transport rates inversion. Uncertainties and further improvements of the method are discussed.

1 Introduction

Direct observational estimates of vertical and lateral turbulent transport rates are largely limited to studies of surface drifter dispersion (e.g. Krauß and Böning, 1987), surface eddy fluxes estimated from satellite data (e.g. Abernathey and Marshall, 2013), occasionally released tracer dispersion (e.g. Ledwell et al., 1993), and rare micro-structure measurements (see Waterhouse et al., 2014). However the vast collection of in situ profiles provided by Argo (Roemmich et al., 1999, 2009) may offer new opportunities to infer turbulent transport rates from the sea surface to 2000 m depth. Inferences of ~~diapycnal diffusivity~~

from Argo profiles diffusivities is possible through the analysis of their fine scale structure (Wu et al., 2011; Whalen et al., 2012) . Furthermore the Argo variance fields combined with conceptual turbulence models (Wu et al., 2011; Whalen et al., 2012; Cole et al., 2015) . The extensive observation of the broad scale broad-scale hydrography characteristics by Argo may also provide a basis for the inversion of turbulent transport rates.

The idea that turbulent transports can be inferred from observed characteristics of the broad scale broad-scale hydrography goes back to Iselin (1936, 1939) and likely even further. It is for example the basis of the Munk (1966) estimate of diapycnal diffusivity from temperature profile curvatures below 1000 m (following upon Wyrtki, 1962). Many subsequent studies have pursued comparable inferences of turbulent transport rates (or parameters) from observed broad scale broad-scale hydrography characteristics using conceptual models as well as general circulation models and adjoint techniques (e.g. Schott and Zantopp, 1980; Walin, 1982; McDougall, 1984; Olbers et al., 1985; Tziperman, 1986; Tomczak and Large, 1989; Ganachaud, 2003; Stammer, 2005; Ferreira et al., 2005; Lumpkin and Speer, 2007; Zika et al., 2009; Liu et al., 2012). The large influence of vertical and lateral turbulence in setting the large-scale characteristics of the ocean state in numerical models (e.g. Danabasoglu and Marshall, 2007; Eden et al., 2009; Griffies et al., 2010; Jochum et al., 2013; Gnanadesikan et al., 2014; Melet et al., 2014) underscores that the large-scale ocean state observation carries a wealth of information on turbulent transport rates.

Despite this long history and strong modeling evidence, it is not clear that inverse parameter estimates are useful, robust and/or physically meaningful. Munk's estimate of diapycnal diffusivity provides an example of the possible downfall of the method (Munk, 1966; Munk and Wunsch, 1998) (Munk 1966 ; see also Munk and Wunsch 1998). Munk's estimate of about $10^{-4}\,\mathrm{m\,s^{-1}}$ that was originally based upon a one-dimensional model of the Pacific led to the search for the "missing mixing" since direct observations of diapycnal mixing in the thermocline were an order of magnitude smaller than Munk's value (Ledwell et al., 1998, 2000). However it is now commonly accepted that neglected physics (e.g. the adiabatic upwelling of North Atlantic Deep Water in the Southern Ocean; Toggweiler and Samuels 1998, Webb and Suginohara 2001) could explain the discrepancy.

Importantly, this example illustrates the difficulty in interpreting inverse parameter estimates, and the possible confusion brought on by assumptions built in the fitted model. In light of the ~~now~~ well documented heterogeneity in ocean mixing rates and processes (reviewed in MacKinnon et al., 2013; Fox-Kemper et al., 2013) the notion that ocean mixing as a whole ~~could~~ can be cast into a one-dimensional model now seems incongruous. Models of extreme simplification, while they can illuminate individual mechanisms, also discount the composite and complex essence of ocean observations.

General circulation models used within a least-squares framework a priori provide a suitable framework to avoid mis-interpreting observations (e.g. aliased small-scale signals) while taking advantage of complementary data sets (e.g. altimetry) and constraints (e.g. atmospheric re-analyses) to infer ~~large scale~~ large-scale ocean balances and diagnose ocean variability (see Wunsch and Heimbach, 2013, for a review). However the few publications that followed this approach to infer turbulent transport parameters (Stammer, 2005; Ferreira et al., 2005; Liu et al., 2012) provide little, if any, evaluation of the method and its results. At best, they point to the usefulness of the estimated parameters in an ad-hoc manner – for example Ferreira et al. (2005) derived a parameterization of eddy diffusivity as a function of stratification that improved the un-constrained ocean model solution.

How many and which degrees of freedom may be well constrained by available observations is just one of the rather technical, yet crucial questions that have never been tackled. Thus one could still argue that parameter inversion (along with forcing fields adjustment) through general circulation models is nothing more than an objective and practical way of tuning these models (i.e. a marginally useful approach). Whether the estimated parameters have any intrinsic value beyond the chosen estimation framework and settings (assimilated observations, period of assimilation, numerical model, etc.) remains unclear just as in the case of conceptual models. Further assessment of data constraints and parameter estimates is clearly needed and equally justified given the obvious importance of the subject matter.

In this paper we aim to demonstrate that extended observation of the ~~broad scale~~ broad-scale hydrography by Argo (see, e.g. Forget and Wunsch, 2007; Forget, 2010; Speer

and Forget, 2013) should translate into improved estimates of upper ocean turbulent transport rates. In other words, we seek to assert that turbulent transport rates are "observable" by means of Argo's collection of temperature and salinity profiles. This is clearly not a trivial proposition given the variety and heterogeneity of oceanic processes intermingled within observational data – especially in the upper ocean. Overarching oceanographic questions regarding the observability of turbulent transport rates by means of ~~broad scale~~ broad-scale measurements largely remain to be answered such as: which specific ~~ocean~~ features of the ocean state are informative of which turbulent transport rates? How precise may inverse estimates of turbulent transport rates be depending on the limited data availability? How are inverse problems best formulated to take full advantage of available observations?

The presented analysis reaches preliminary answers to these open questions, while providing clear supporting evidence that observations of the large-scale ocean stratification by Argo yield useful constraints to estimate turbulent transport parameters, and establishing a frame of reference for further research into their observability. It focuses on the Forget et al. (2015) ocean state estimate over 1992–2011 covering the Argo era and mainly on the 0–2000 m oceanic layer that Argo observes extensively. In this framework, vertical and lateral turbulent transport parameters are estimated by fitting the simulated large-scale ocean state to observations (notably Argo ~~T and S profiles~~ profiles of temperature and salinity). Even though minimal constraints are imposed on the parameters themselves, their geography and impacts are found to be physically meaningful and shown to be useful beyond the estimation procedure.

Section 2 summarizes the estimation method, establishes that the estimated parameters are broadly consistent with the observed large-scale ocean state, and shows that they ~~reduces~~ reduce spurious model drifts using independent ~~bio-geochemistry~~ biogeochemistry data. Section 3 demonstrates the high sensitivity of the observed upper-ocean stratification to the estimated parameters. This result provides clear supporting evidence that Argo profile collections yield a useful observational constraint of regional turbulent transport rates. The estimated turbulent parameters themselves and their relationship to the ~~large scale~~ large-scale ocean state are discussed in Sect. 4. Section 5 provides a discussion of the

uncertainties ~~of~~ in the approach. The findings are summarized and perspectives are drawn in Sect. 6.

2 Reduced model errors

The "Estimating the Circulation and Climate of the Ocean version 4" (ECCO v4) estimate of the evolving ocean state over the period 1992–2011 ~~and~~ as well as the associated model and estimation settings are presented in detail in Forget et al. (2015). In summary, the 20 year solution of the global one degree resolution model is fitted to a suite of data constraints, including the vast collection of Argo profiles of temperature (T) and salinity (S), through iterative adjustments of turbulent transport parameters (time-invariant), atmospheric forcing fields ~~and the 1992 initial conditions~~ (bi-weekly) and initial conditions (on 1992/01/01). Forget et al. (2015) show that the turbulent transport parameter adjustments are particularly important to the close fit of ECCO v4 to observed in situ profiles. They allow a clear reduction in widespread misfits in ECCO v4 (Fig. 1; top left panel) as compared with (1) earlier ECCO solutions that ~~, while optimizing initial conditions and forcing fields , did not optimize~~ optimized surface forcing fields but not turbulent transport parameters (~~the four panels in the~~ top right corner panels) and (2) ~~and as compared with~~ ECCO2 eddying model simulations (bottom three panels).

The turbulent transport parameters being estimated, and the focus of this paper, are time-invariant three dimensional maps of bolus velocity coefficient $\mathcal{K}_{\mathrm{gm}}$ (Gent and Mcwilliams, 1990), isopycnal diffusivity $\mathcal{K}_\sigma$ (Redi, 1982), and background diapycnal diffusivity $\mathcal{K}_{\mathrm{d}}$ (aside from mixed layer parameterizations). The tendency equation for a tracer ϕ in the ocean interior can thus be written in simplified form as:

$$\frac{\partial \phi}{\partial t} + \nabla \cdot (\boldsymbol{u}\,\phi + \boldsymbol{u}^\star\,\phi) = \nabla \cdot (\mathcal{K}_\sigma \nabla_\sigma \phi) + \frac{\partial}{\partial z}\left(\mathcal{K}_z \frac{\partial \phi}{\partial z}\right), \tag{1}$$

where $\mathcal{K}_z$ includes $\mathcal{K}_{\mathrm{d}}$ plus contributions from mixed layer parameterizations ~~(Gaspar et al., 1990; Duffy et al., 1999, plus simple convective adjustment) ,~~

(Gaspar et al. 1990 , Duffy et al. 1999 , plus simple convective adjustment), $\nabla_\sigma \phi$ is the lateral tracer gradient on isopycnal surfaces (Redi, 1982), $\boldsymbol{u}$ is the Eulerian velocity, and $\boldsymbol{u}^\star$ is the parameterized bolus velocity representing the advective (adiabatic) effect of ~~mesoscale~~ meso-scale eddies. After Gent and Mcwilliams (1990) the ~~(~~non-divergent ~~)~~ bolus velocity is evaluated as $\boldsymbol{u}^\star = -\nabla \times \Psi^\star$ where $\Psi^\star = (\mathcal{K}_{\rm gm} S_y, \mathcal{K}_{\rm gm} S_x, 0)$ is the bolus streamfunction, and S_x and S_y are the isopycnal slopes in the zonal and meridional directions, respectively.

The first guess values are the constants $K_{\rm gm} = 10^3$, $K_\sigma = 10^3$ and $K_{\rm d} = 10^{-5}\,{\rm m^2\,s^{-1}}$ with respective uncertainties set to $u_{\rm gm} = 500$, $u_\sigma = 500$ and $u_{\rm d} = 10^{-4}$ ${\rm m^2\,s^{-1}}$. As part of ECCO v4, the specification of error covariances for $\mathcal{K}_{\rm gm}$, $\mathcal{K}_\sigma$ and $\mathcal{K}_{\rm d}$ is limited to imposing smoothness at the scale of three grid points, thus allowing regional adjustments to emerge simply from observational constraints under the dynamical model constraint. The respective ranges of permitted adjustment are $10^2 < \mathcal{K}_{\rm gm} < 10^4$, $10^2 < \mathcal{K}_\sigma < 10^4$, and $10^{-6} < \mathcal{K}_{\rm d} < 5 \times 10^{-4}\,{\rm m^2\,s^{-1}}$. The specified ranges span values found (directly or indirectly) in observations as well as values typically used in general circulation models.

Note that the constraints imposed specifically on the turbulent parameters (smoothness and range) are minimal on purpose. One could envision imposing further constraints, for example on the vertical ~~profiles or the energetic~~ structure or the energetics of the turbulent parameters. Here, instead, the turbulent parameters can adjust freely within the specified ranges that reflect their large a priori uncertainty at the scale of a few grid points. Accordingly, the adjusted parameters spread out over the specified ranges as a result of observational constraints being imposed (Fig. 2). The ~~particularly large adjustments seen in the top 2000that Argo observes readily points to the importance of this dataset (Fig. 2). The geography of parameter adjustments dictated by data constraints is further assessed in~~ primary objective of this paper is to reveal the observational basis to these adjustments being provided by the rapidly growing in-situ data base (Sects. 3 and ~~4.~~ 4).

To test the estimated turbulent parameters beyond the 20 years of the estimation window, two ~~500~~model integrations are carried out for 500 years that perpetually loop over the 1992–2011 forcing of the ECCO v4 state estimate. One integration uses the estimated

parameters while the other uses the constant first guess parameters (which, we should underscore, are common values used in ocean models of comparable horizontal resolution). The turbulent transport parameter adjustments yield a clear reduction in the model's tendency to drift away from observations over multiple centuries (Fig. 3). This is true not only for the physical variables that were directly constrained by Argo profiles (left panels) but also for ~~bio-geochemical~~ biogeochemical variables that were not (middle and right panels).

The ~~bio-geochemistry~~ biogeochemistry result is most remarkable as it provides independent evidence that the turbulent transport parameter adjustments as estimated from observations of physical variables reduce internal model error more generally. In itself this novel result demonstrates strong constraints imposed (directly or indirectly) by observations of the physical state on ~~bio-geochemistry. Whether it is primarily due to $\mathcal{K}_{\mathrm{gm}} - K_{\mathrm{gm}}$, $\mathcal{K}_\sigma - K_\sigma$ and $\mathcal{K}_{\mathrm{d}} - K_{\mathrm{d}}$ appearing in the bio-chemical tracer equations or rather results from improved physical variables (T, S, $\boldsymbol{u}$ and dependent variables that impact biochemistry) is an interesting question left for further investigation. But in any event the~~ biogeochemistry. The resulting improvement in ~~bio-geochemistry~~ biogeochemistry (Fig. 3) implies that regional turbulent transport rates are at least partly observable by available observations of physical variables. It further motivates the assessment of the estimated turbulent transport parameters and of their observational basis presented ~~in Sects. 3 and 4.~~ below.

Before returning the focus to the 20 year estimation period, it is worth illuminating the consequences of $\mathcal{K}_{\mathrm{gm}}$, $\mathcal{K}_\sigma$ and $\mathcal{K}_{\mathrm{d}}$ over longer time scales (Fig. 4). The fact that the benefits of the ocean state estimation procedure extends much beyond its 20 years (Fig. 3) and through the abyss over centennial time scales (not shown) is indeed clearly not a trivial result. It implies dramatic changes in the formation and ventilation of oceanic water masses, as demonstrated by zonal mean oxygen concentrations after 500 years (Fig. 4).

The fact that the ECCO v4 turbulent transport ~~parameters adjustment~~ parameter adjustments (Fig. 2) ~~increases~~ increase the simulated oxygen concentration in the subtropical abyss (Fig. 4) in particular denotes an intensification in the formation and spreading of Antarctic Bottom Water (also evident near Antarctica at all depths). The improved ~~maintaining~~ maintainance of a high oxygen content in the Arctic and of the mid-latitude oxy-

gen minimum region is equally remarkable (Fig. 4). While the oxygen minimum exists due to oxygen consumption by ~~bio-geochemistry~~biogeochemistry, it is also largely shaped by physical processes (Wyrtki, 1962)~~, and~~ . Fig. 4 provides ~~strong~~ evidence that it is ~~indeed~~ effectively constrained by Argo's collection of T and S profiles ~~.~~ via their constraint of turbulent transport parameters revealed in Sects. 3 and 4. Whether the constraint of the oxygen minimum results directly from $\mathcal{K}_{\mathsf{gm}} - K_{\mathsf{gm}}$, $\mathcal{K}_\sigma - K_\sigma$ and $\mathcal{K}_{\mathsf{d}} - K_{\mathsf{d}}$ appearing in the biogeochemical tracer equations or rather indirectly from improvements in other physical variables (T, S, etc.) impacting biochemistry is an interesting question left for further investigation.

3 Parametric controls of ocean stratification

The new constraints on turbulent transport parameter inversions brought by data collected over the past decade can most immediately be gauged using linear adjoint sensitivities (Fig. 5 for $\mathcal{K}_{\mathsf{gm}}$). The results show that the constraint provided by one decade of Argo data collection (bottom) generally exceeds that provided by two decades of altimetry (middle). Furthermore, the large sensitivity increase seen upon moving from the top panel (10 years of altimetry) to the middle panel (20 years of altimetry) illustrates how the second decade of Argo data collection should even further solidify the observational basis to turbulent transport parameter inversions. These considerations motivate the detailed investigation of the existing Argo data constraint presented below.

The geography and values of ocean stratification ($\frac{\partial \rho}{\partial z}$ and mixed layer depths) are a priori particularly relevant to turbulent transport rate inferences. Stratification is indeed a prime candidate amongst observational constraints as it is intimately related to potential vorticity, water mass formation and ventilation, which in turn strongly constrain the general ocean circulation (see e.g. Walin, 1982; Luyten et al., 1983). ~~Furthermore~~ Argo's collection of T and S profiles yields an extensive observation of ocean stratification (Fig. 6). Its importance as an observational constraint of $\mathcal{K}_{\mathsf{gm}}$, $\mathcal{K}_\sigma$ and $\mathcal{K}_{\mathsf{d}}$ is established below.

At 300 m outside of the tropics, lows in $\frac{\partial \rho}{\partial z}$ (Fig. 6, bottom left) delineate regions of deep winter convection (Fig. 6, bottom right) and mode water formation (see Speer and Forget, 2013). In the tropics at 300 m, lows in $\frac{\partial \rho}{\partial z}$ denote thermoclines shallower than 300 m. Conversely, subtropical and tropical thermoclines intersecting 300 m are marked by highs in $\frac{\partial \rho}{\partial z}$ (Fig. 6, bottom left). The state estimate's stratification geography and values (Fig. 6, middle left) generally are in very good agreement with Argo observations (Fig. 6, bottom left). Thus the estimated $\mathcal{K}_{\mathrm{gm}}$, $\mathcal{K}_{\sigma}$ and $\mathcal{K}_{\mathrm{d}}$ are consistent with the observed stratification.

To evaluate the full non-linear sensitivity of ocean stratification to each of the three parameters, three forward perturbation experiments are conducted. In each experiment on parameter is individually reset to its constant first guess value. It is worth recalling that atmospheric forcing field adjustments (in temperature, specific humidity, downward radiation, precipitation, and wind stress) have a lesser impact on the subsurface hydrography than turbulent transport parameter adjustments do in ECCO v4 (Forget et al., 2015). In particular it is readily evident in Fig. 6 that the realism of the state estimate stratification is ~~largely due to $\mathcal{K}_{\mathrm{gm}}$, $\mathcal{K}_{\sigma}$ and $\mathcal{K}_{\mathrm{d}}$~~ noticeably improved by the turbulent transport parameter adjustments (compare middle and top panels). Therefore the adjusted atmospheric forcing fields are retained in all perturbation experiments presented here to focus on turbulent transport parameters and their observability.

~~To evaluate the sensitivity of ocean stratification to each estimated parameter, a perturbation experiment is conducted in which it ($\mathcal{K}_{\mathrm{gm}}$, $\mathcal{K}_{\sigma}$ or $\mathcal{K}_{\mathrm{d}}$) is reset to its constant first guess value (K_{gm}, K_{σ} or K_{d}).~~ The mean squared deviation of $\frac{\partial \rho}{\partial z}$ between each perturbed solution and the state estimate over the period 2008–2010, normalized by the corresponding $\frac{\partial \rho}{\partial z}$ variance, is shown in logarithmic scale as a function of latitude and depth (Fig. 7). Logarithmic values above 0 indicate $\frac{\partial \rho}{\partial z}$ contrasts between solutions being as large as the zonal and seasonal mean $\frac{\partial \rho}{\partial z}$ variance in the state estimate. Such large impact of turbulent transport parameter adjustments on $\frac{\partial \rho}{\partial z}$ occurs at all latitudes in the upper 2000 m.

Figure 7 thus provides decisive supporting evidence ~~in favor of the defended observability proposition – it reveals~~ that inversion of regional turbulent transport rates is effectively

guided by the constraint of fitting Argo profiles~~of T and S~~. The collocation of large ocean stratification changes (Fig. 7) and turbulent transport parameter adjustments (Fig. 2) further confirms that they are tied to each other in ECCO v4 (see Sect. 4 for more detail).

Generally in the upper 2000 m and over the whole water column at high latitudes, ocean stratification is found to be more sensitive to $\mathcal{K}_{\text{gm}}$ (Fig. 7, top) than to $\mathcal{K}_\sigma$ (middle) or $\mathcal{K}_{\text{d}}$ (bottom). The predominant impact of $\mathcal{K}_{\text{gm}}$ suggests that ocean stratification profiles may most efficiently constrain (i.e. observe) the rates of bolus advection, albeit with several noteworthy exceptions. High sensitivity to $\mathcal{K}_\sigma$ (Fig. 7, middle) is found at high latitudes. The impact of $\mathcal{K}_\sigma$ on $\frac{\partial \rho}{\partial z}$ is indirect since $\nabla_\sigma \phi$ in Eq. (1) vanishes for $\phi = \sigma$. It does however have dynamical impacts and it is not surprising that they are magnified at high latitudes where dense layers outcrop and interact with mixed layer and sea-ice processes (e.g. see England, 1993; Zika et al., 2009). Furthermore haline density variations overcome thermal density variations at those latitudes (e.g. see Forget and Wunsch, 2007; Forget and Ponte, 2015) and this transition provides an environment conducive to dynamical impacts of $\mathcal{K}_\sigma$. High sensitivity to $\mathcal{K}_{\text{d}}$ is found in the tropics and in the Arctic in the 0–2000 m layer, as well as near the sea surface at all latitudes. This result implies that ~~Argo's~~ observation of the stratification ~~broad structure~~ broad-structure informs us of diapycnal diffusion rates in these regions.

Winter mixed layers modulate water mass transformations and the penetration of surface buoyancy fluxes. As such they are a key factor in ocean stratification and deserve special attention. The state estimate closely agrees with the geography and magnitude of observed mixed layers (Fig. 6, right panels). The sensitivity of mixed layer depths to turbulent transport parameters (Fig. 8) varies on a regional basis and mostly reflects the underlying stratification sensitivity (Fig. 7). Logarithmic values above 0 in Fig. 8 indicate that changes in mixed layer depths that result from the parameter adjustments are as large as the seasonal contrasts seen in the state estimate. Such differences in mixed layer depths provide additional evidence of efficient constraints imposed by Argo on turbulent transport rates.

Several dynamical regimes can be distinguished in Figs. 7 and 8 that are in broad agreement with theoretical views and worth commenting upon before proceeding with further assessment of the geography (Sect. 4) and uncertainty (Sect. 5) of $\mathcal{K}_{\rm gm}$, $\mathcal{K}_\sigma$ and $\mathcal{K}_{\rm d}$.

The thermocline in the upper 2000 m (between 60° S and 60° N) is primarily adjusted through adiabatic circulation controls (Fig. 7, top panel) rather than diapycnal mixing changes (Fig. 7, bottom panel). This behavior is prompted by data constraints leading to $\mathcal{K}_{\rm gm}$, $\mathcal{K}_\sigma$ and $\mathcal{K}_{\rm d}$ rather than by a priori assumptions. Thus, Fig. 7 provides objective observational support for predominantly adiabatic, ventilated thermocline theories (see Vallis, 2006).

The sizable impact of the increased $\mathcal{K}_{\rm d}$ at the base of the ventilated thermocline further supports the notion that it is embedded in an internal thermocline (Samelson and Vallis, 1997) where diffusion balances advection (see Figs. 2 and 7). Another regime appears near the sea surface in the tropics, where shallow mixed layers and stratification also strongly respond to background diapycnal mixing (Figs. 7–8). Finally, high latitudes where deep isopycnals outcrop and experience large isopycnal variations in T and S expectedly show a sizable impact of $\mathcal{K}_\sigma$, along with the predominant impact of $\mathcal{K}_{\rm gm}$ (Figs. 7–8). The existence of such contrasting dynamical regimes points to the importance of not overly simplifying the inversion problem and the underlying model.

4 Estimated turbulent transport parameters

The ~~defended observability proposition implies~~ results from Sects. 2 and 3 suggest that the estimated $\mathcal{K}_{\rm gm}$, $\mathcal{K}_\sigma$ and $\mathcal{K}_{\rm d}$ may have oceanographic value beyond the ECCO v4 state estimate itself – a notion supported by Fig. 3 in particular. The main goal of this section is to further assert the relationship between the observed ocean stratification and estimated turbulent transport parameters, and to assess ~~that~~ whether the estimated parameter maps are ~~indeed~~ physically meaningful.

Each of the estimated parameters varies by orders of magnitudes on a regional basis, and thus shows a great degree of heterogeneity (Fig. 9) – a physically reasonable propo-

sition (see, e.g. Eden, 2006; Eden et al., 2007; Fox-Kemper et al., 2013). Highs and lows often alternate at the same latitudes over extended regions. $\mathcal{K}_{\mathsf{gm}}$, $\mathcal{K}_\sigma$ and $\mathcal{K}_{\mathsf{d}}$ however also show extended regions of limited departure from K_{gm}, K_σ and K_{d} (regions in green). This behavior ought to be expected in regions where turbulent transports may be weak regardless of the corresponding coefficients.

Patterns of large parameter adjustments generally align with contours of observed stratification (Fig. 9). Stratification contrasts are indeed expected to delineate between regimes of turbulence, where one or another physical process may become predominant. Parameterized turbulent transports furthermore act along or across isopycnals, and stratification contrasts are indicators of the isopycnals geography.

Parameterized advection of tracers by meso-scale eddies (see Eq. 1) is controlled by $\mathcal{K}_{\mathsf{gm}}$. Reduction in $\mathcal{K}_{\mathsf{gm}}$ is most distinctly seen at the equatorward flank of the subtropical thermocline bowl in all oceanic basins (Fig. 9, top). Low $\mathcal{K}_{\mathsf{gm}}$ values appear consistent with the observed tropical thermocline characteristics (Figs. 1 and 6). The tropics are indeed known to show relatively low levels of meso-scale eddy activity and a predominance of baroclinic wave trains instead (e.g. Tulloch et al., 2009). The decrease from K_{gm} to $\mathcal{K}_{\mathsf{gm}}$ acts to increase the equatorward slant of isopycnals per Eq. (1).

Instances of $\mathcal{K}_{\mathsf{gm}} \geq K_{\mathsf{gm}}$ are common at higher latitudes where large isopycnal slopes are found. $\mathcal{K}_{\mathsf{gm}} > K_{\mathsf{gm}}$ is found at subpolar latitudes and not necessarily at the cores of the Antarctic Circumpolar Current (ACC) and subtropical jets~~– a proposition that can be defended on theoretical grounds (see Marshall et al., 2006, and references therein) .~~. We refer the reader to Ferreira et al. (2005) and Liu et al. (2012) for discussions of comparable results. Following the various ACC branches and meanders, instances of both $\mathcal{K}_{\mathsf{gm}} < K_{\mathsf{gm}}$ and $\mathcal{K}_{\mathsf{gm}} > K_{\mathsf{gm}}$ are found depending on longitude, as should be expected from Eden (2006) and subsequent studies. Furthermore, vertical contrasts in $\mathcal{K}_{\mathsf{gm}}$ are readily apparent in Fig. 9, such as the appearance of $\mathcal{K}_{\mathsf{gm}} > K_{\mathsf{gm}}$ patches in the ACC between 300 and 900 m depth. They become even more predominant at greater depths (see Sect. 5).

Isopycnal tracer diffusion due to lateral turbulence is controlled by $\mathcal{K}_\sigma$ (see Eq. 1). Similar adjustment patterns can be seen in $\mathcal{K}_\sigma$ (Fig. 9, middle) and $\mathcal{K}_{\mathsf{gm}}$ (Fig. 9, top). Notably

$\mathcal{K}_\sigma$ ~~and $\mathcal{K}_{\mathrm{gm}}$ consistently show low values~~ shows minima in the tropics at 300m and below (in qualitative agreement with Cole et al., 2015) that correspond to $\mathcal{K}_{\mathrm{gm}}$ minima (see also Fig. 2). This is not entirely surprising since the two paramaterized processes, while generally distinct, are both associated with lateral turbulence, so that $\mathcal{K}_\sigma$ and $\mathcal{K}_{\mathrm{gm}}$ may covary (see, e.g. Abernathey et al., 2013). It should be noted however that the estimation settings did not impose covariance between the two parameters, but it is allowed to emerge from data constraints if adequate. Differences between $\mathcal{K}_\sigma$ and $\mathcal{K}_{\mathrm{gm}}$ could conversely indicate regions where the ocean state is not equally sensitive to the diffusive and advective effects of lateral turbulence.

One notable feature in $\mathcal{K}_\sigma$ (Fig. 9, middle right) that is not in $\mathcal{K}_{\mathrm{gm}}$ (Fig. 9, top right) is its reduction from K_σ near 900 m on the southern side of the ACC and near Antarctica (see also Fig. 2). It is physically reasonable that isopycnal diffusion is a particularly sensitive process in regions showing large tracer gradients along isopycnals (see Gnanadesikan et al., 2014). Also notable are two contrasting situations in the North Atlantic. The subpolar gyre shows increased $\mathcal{K}_{\mathrm{gm}}$ and $\mathcal{K}_\sigma$. The eastern subtropics at 900 m (near the Mediteranean outflow depth) show reduced $\mathcal{K}_{\mathrm{gm}}$ but increased $\mathcal{K}_\sigma$. As emphasized by Abernathey et al. (2013), $\mathcal{K}_{\mathrm{gm}}$ and $\mathcal{K}_\sigma$ are not expected to be equal except under specific limits. Gnanadesikan et al. (2014) further illustrate that tying $\mathcal{K}_\sigma$ strictly to $\mathcal{K}_{\mathrm{gm}}$ (as is often done in ocean modeling) can be problematic. The contrasted cases seen in Figs. 2 and 9 provide observational evidence that $\mathcal{K}_\sigma$ and $\mathcal{K}_{\mathrm{gm}}$ are not systematically tied to each other.

Background diapycnal diffusivity $\mathcal{K}_{\mathrm{d}}$ is increased from K_{d} at 300 m near 30° latitude (Fig. 9, bottom left). This geography qualitatively agrees with the ~~fine structure~~ fine-structure observed by Argo (Fig. 1 in Whalen et al., 2012) and theoretical predictions of intensified parametric subharmonic instability (e.g. MacKinnon and Winters, 2005). However interleaving of weak and strong mixing layers is a common feature of the $\mathcal{K}_{\mathrm{d}}$ inverse estimate. Hence $\mathcal{K}_{\mathrm{d}}$ at 900 m (Fig. 9, bottom right) is rather reduced at 30° latitudes.

A pronounced interleaving is also seen in $\mathcal{K}_{\mathrm{d}}$ near the Equator (Fig. 10). Increased $\mathcal{K}_{\mathrm{d}}$ in the upper 100 m is consistent with the analysis of (amongst others) Moum et al. (2009) and found in all basins. A secondary $\mathcal{K}_{\mathrm{d}}$ maximum can be seen in the Pacific and Atlantic

immediately underneath the Equatorial Under Curent. Shear instability is a good candidate mechanism also in this case. The deepest Pacific maximum (near 1000 m in Fig. 10) is a tropical rather than equatorial feature (Fig. 9, bottom right). Its dynamical origin is likely very different from the two upper maxima, and associated with the internal thermocline (see Sect. 3; Fig. 7).

In summary this section shows that the regional contrasts in $\mathcal{K}_{\rm gm}$, $\mathcal{K}_\sigma$ and $\mathcal{K}_{\rm d}$ are tied to regional stratification contrasts, and that these estimates generally are physically plausible. It is not implied however that turbulent transport rates are uniquely dependent on stratification alone and everywhere. The interplay of instability processes that in turn govern turbulent transports and stratification on a regional basis certainly remains a subject of active research of great importance beyond this paper. The presented analysis simply supports the notion that turbulent transport rates are effectively constrained (i.e. observable) by means of Argo's extensive collection of stratification profiles.

5 Assessment of uncertainties

~~The goal here is to gauge turbulent transport parameter uncertainties, by assessing similarities anddifferences amongst published inversion results (Ferreira et al., 2005; Stammer, 2005; Liu et al., 2012, along with ECCO v4)~~ A comparison of ECCO v4 parameter estimates (Figs. 9 and 11) with earlier inversion results that did not cover the Argo era (Ferreira et al., 2005; Stammer, 2005; Liu et al., 2012) should be indicative of overall observational uncertainty levels. None of the listed estimates is provided with a formal error estimate, which more generally remains a major caveat of ocean modeling and data synthesis. In such context inter-comparison of solutions is a commonly accepted, practical method to assess uncertainties even though its results are often difficult to interpret precisely (see Danabasoglu et al., 2014; Balmaseda et al., 2014). ~~Attributing specific differences amongst the four~~

In particular, attributing point by point differences amongst inverse estimates to specific causes would be a perilous exercise~~(as they differ in a number of potentially important~~

aspects of the , due to various differences in model and estimation settings) , and therefore no such attempt is made. However comparing the earlier inverse estimates with ECCO It is worth highlighting, however, that ECCO v4 that further covers the Argo era through 2011 should be indicative of overall observational uncertainty levels. benefits from many innovations (e.g., updated numerics, the addition of a sea ice model and of the Arctic, and increased vertical resolution) as compared with previous generation model setups used by Ferreira et al. (2005) , Stammer (2005) , and Liu et al. (2012) . A more exhaustive list of innovations is provided by Forget et al. (2015) .

It

The most meaningful comparison maybe between the ECCO v4 and Liu et al. (2012) results since their respective experimental settings are most comparable. Importantly, estimated parameter adjustments are larger in ECCO v4 than in Liu et al. (2012) (compare Fig. 11 with Figs. 7c, 12b and 13b in Liu et al. 2012). It should be noted that the impact of the K_{gm}, K_{σ} and K_{d} adjustments in ECCO v4 was shown to generally exceed the impact of model errors unrelated to turbulent transport parameterizations (Forget et al., 2015) . Therefore the increased parameter adjustment amplitude (in ECCO v4 as compared with Liu et al. 2012) is thought to primarily reflect the extensive data constraints added over 2002-2011 (see Fig. 5) rather than differences in model settings.

Regardless of the noted caveats, it is encouraging that the presented turbulent transport ECCO v4 parameter estimates (Figs. 9 and 11) bear some resemblance to the Ferreira et al. (2005); Stammer (2005) Ferreira et al. (2005) , Stammer (2005) and Liu et al. (2012) results, as it which may indicate robust oceanic features. All estimates are rich in regional adjustment patterns aligned with contours of the large scale hydrography. All large-scale hydrography. The three $\mathcal{K}_{\mathrm{d}}$ estimates (Stammer, 2005; Liu et al., 2012 and ECCO v4) show elevated mixing near 30° latitude at 300 m, and interleaving of high and low mixing in the tropics. The $\mathcal{K}_{\mathrm{d}}$ map of Liu et al. (2012) at 300 m (their Fig. 7a) more generally is in a good qualitative agreement with Fig. 9 (bottom left). The three estimates of As a final example the three $\mathcal{K}_{\mathrm{gm}}$ estimates (Ferreira et al., 2005; Liu et al., 2012 and

ECCO v4) show maxima associated with the ACC~~. Both Ferreira et al. (2005) and ECCO v4 show much reduced $\mathcal{K}_{gm}$~~, minima in the tropics, ~~where Liu et al. (2012) also tends towards reduced $\mathcal{K}_{gm}$, and all three estimates show increased $\mathcal{K}_{gm}$~~ and maxima in the North Atlantic subpolar gyre.

~~However, major differences arealso found~~ There are, however, also many differences amongst inverse parameter estimates. ~~For example, Liu et al. (2012) find relatively small $\mathcal{K}_{gm}$ adjustments~~ Firstly, ECCO v4 shows intensified diapycnal mixing in the tropical thermocline below 500m (Fig. 11; bottom panel) as compared with ~~Ferreira et al. (2005) and ECCO v4, as well as relatively small $\mathcal{K}_d$ adjustments below 300depth. The three estimates of~~ Stammer (2005) and Liu et al. (2012) . Secondly, the three $\mathcal{K}_{gm}$ ~~in~~ estimates largely differ in their magnitude and vertical structure in the ACC and at 40° N~~also differ in their magnitude and vertical structure~~. Ferreira et al. (2005) show increased $\mathcal{K}_{gm}$ in the upper 1000 m in the ACC, with a near surface maximum~~., whereas~~ Liu et al. (2012) and ECCO v4 ~~rather~~ (Fig. 11; top panel) show increased $\mathcal{K}_{gm}$ between 1000 and 3000 m~~(Fig. 11).~~ . In the Gulf Stream, Ferreira et al. (2005) show a $\mathcal{K}_{gm}$ maximum in the upper 1000 m, ~~while Liu et al. (2012) show a $\mathcal{K}_{gm}$ minimum, and ECCO~~whereas Liu et al. (2012) and ECCO v4 ~~is neutral (Fig. 11). Finally~~show $\mathcal{K}_{gm}$ minima at these depths. Also, neither Ferreira et al. (2005) nor Liu et al. (2012) show the increased $\mathcal{K}_{gm}$ seen near the coast ~~Antarctica seen in~~ of Antarctica in ECCO v4. Finally, K_σ in ECCO v4 (Fig. 11; middle panel) hints at a steering level effect (Green, 1970; Abernathey et al., 2010; Ferrari and Nikurashin, 2010) below 500m in the ACC that is not seen in Liu et al. (2012) . Such differences are indicative of large overall uncertainty in inverse parameter estimates.

Furthermore, regions where parameters remain virtually unadjusted (Figs. 2 and 9; regions in green) ~~a priori denote large parameter uncertainty when none of the included observational constraints is sufficiently~~ likely denote large uncertainties reflecting that available data constraints are insufficiently sensitive to prompt sizable parameter adjustments (as noted by Liu et al., 2012). ~~In this regard the~~ The relatively weak values of $\mathcal{K}_d - K_d$ in the ACC (as compared with, e.g., Whalen et al. 2012 , but not with Liu et al. 2012) may

be one example. Similarly the fact that $\mathcal{K}_\mathrm{d} - K_\mathrm{d}$ is generally muted in the abyss (albeit with notable exceptions in the Southern Ocean) is not surprising, and does not imply that K_d is a precise first guess. Indeed the equilibration of the abyssal stratification (or the lack thereof) and the recycling of abyssal water masses are dominated by very long time scales, and abyssal observations are very sparse as compared with upper ocean data constraints.

It is in fact encouraging that $\mathcal{K}_\mathrm{d}$ shows even marginal increases near the sea floor (Figs. 12, right and 2, bottom right) as it is often expected to result from the interaction of barotropic tides (amongst others) and bottom topography (Polzin et al., 1997; Ledwell et al., 2000; Naveira Garabato et al., 2004; Sloyan, 2005). It is intriguing that low K_d values are also found near the bottom – mostly in the Southern Ocean along deep canyon margins (Figs. 12, right and Fig. 2, bottom left). However reductions in diapycnal diffusivity (from K_d to $\mathcal{K}_\mathrm{d}$) may compensate for an unknown amount of numerical diffusion implied by the advection schemes, and bottom boundary layers are notoriously difficult to simulate adequately in ocean models. For these reasons, and since they are not seen in Stammer (2005) or Liu et al. (2012), the $\mathcal{K}_\mathrm{d}$ contrasts in Fig. 12 should be interpreted most cautiously.

The deep Southern Ocean can adjust relatively fast due to the proximity of bottom water formation sites and the presence of a deep wind- and eddy-driven thermocline (see Karsten and Marshall, 2002) that result in a strong coupling of superficial and deep layers in the ACC region (see Fig. 7). Hence the large values of $\mathcal{K}_\mathrm{gm}$ at 3000 m estimated over 20 years in the Southern Ocean may be physically meaningful (Fig. 12, left). Maxima in $\mathcal{K}_\mathrm{gm}$ are located along the ACC path just downstream of Kerguelen and at Drake passage, as well as in the Brazil–Malvinas confluence region, in the Ross Sea and in the Weddell Sea. These regions are indeed characterized by relatively large isopycnal slopes, and eddying numerical models show sizable meso-scale eddy activity even at 3000 m along the ACC (Ponte, 2012). It will be interesting to see whether the $\mathcal{K}_\mathrm{gm}$ maxima seen in Fig. 12 are confirmed (or otherwise) in inversion experiments conducted once deep Argo profiles are available.

6 Summary and perspectives

This study asserts that extended observation of the ~~broad scale~~ broad-scale hydrography by Argo should translate into improved inverse estimates of regional turbulent transport rates in the upper 2000 m over the global ocean. Time-invariant three-dimensional maps of turbulent transport parameters ($\mathcal{K}_{\mathrm{gm}}$, $\mathcal{K}_{\sigma}$ and $\mathcal{K}_{\mathrm{d}}$) are estimated as part of ECCO v4 (Forget et al., 2015) and under the observational constraint of Argo T-S profiles collected through 2011. The presented exploration of the method of turbulent transport parameter inversion, while still incomplete, fills a major gap in the oceanographic literature.

The observability of turbulent transport rates is asserted by focusing on ocean stratification ($\frac{\partial \rho}{\partial z}$ and mixed layer depths). Argo indeed readily observes these key oceanographic variables with un-precedented data coverage. The estimated turbulent transport parameters are consistent with the observed stratification by construction, since it is well reproduced by the ECCO v4 ocean state estimate. It is shown that ocean stratification over the upper 2000 m is highly sensitive to the estimated parameter adjustments, and that the geography of estimated parameter adjustments is aligned with contours of observed ocean stratification. Thus, the constraint of fitting Argo profiles is identified as an effective observational basis for the inversion of turbulent transport parameters.

As part of the inversion method evaluation it is shown that the estimated parameters reduce spurious model drifts (i.e. accumulating model biases) of the physical ocean state in multi-century simulations. They also lead to remarkable improvements in simulating ~~bio-geochemistry~~ biogeochemistry variables that were not involved in the parameters optimization. The estimated parameter adjustments themselves and the resulting adjustments in ocean stratification are physically plausible despite the minimal constraints that were built in the optimization. These results demonstrate that the estimated parameters have intrinsic value beyond the optimized solution of the 20 year evolving ocean physical state.

The asserted "observability" of turbulent transport rates by Argo does not, however, require or imply that the present parameter estimates are very precise or accurate. Given the noted contrasts amongst published inversion results, and given that vast regions show

negligible parameter adjustments, it is unlikely that available T-S profiles suffice to determine regional turbulent transport rates uniquely and everywhere. The overall weakness of estimated parameter adjustments in the abyss is also revealing of current limitations – extensive Argo data collection has only reached 2000 m and 20 years is too short to fully resolve (im)balances of the abyss. Additional observational constraints (e.g. passive and ~~bio-geo-chemical~~ biogeochemical tracer observations), statistical constraints (e.g. observed ~~fine scale~~ fine-scale and meso-scale statistics) and dynamical constraints (e.g. longer time scales, energetics) ought to complement the constraint of T-S profiles in future inversion experiments.

The lack of a practical technology to associate estimated turbulent transport parameters with formal error estimates is arguably the main caveat here as well as in ~~Stammer (2005); Ferreira et al. (2005)~~ Stammer (2005) , Ferreira et al. (2005) , and Liu et al. (2012). It is the reason why observability of turbulent transport rates by means of Argo and other global data sets largely remains to be quantified. The presented inter-comparison of inversion results, however, provides clues into overall levels of uncertainty. The closest agreement appears to be between $\mathcal{K}_{\mathrm{d}}$ estimates at 300 m. A much more contrasted picture emerges for e.g. $\mathcal{K}_{\mathrm{gm}}$ in the main mid-latitude jets (ACC, Gulf Stream, Kuroshio). ~~While the~~ The three inverse estimates of $\mathcal{K}_{\mathrm{gm}}$ (Ferreira et al., 2005; Liu et al., 2012; Forget et al., 2015) show both minima and maxima along or near the jets, ~~they indeed differ~~ but with differences in their geographic and vertical distributions.

Aside from the need for formal error estimates, and additional constraints, much remains to be done to refine inverse estimates of turbulent transport rates, and our understanding of their observability. One practical approach would consist in conducting twin estimation experiments (see, e.g. Forget et al., 2008a) focusing on turbulent transport parameter inversions. Another one would consist in conducting dedicated estimation experiments where real data ~~is~~ sets are withheld or added one at a time to further compare the constraints that they respectively provide (see, e.g. Forget et al., 2008b). And the presented results should eventually be re-evaluated on the basis of additional estimation experiments that would dif-

fer from Forget et al. (2015) in regard of parameter ranges, first guess values, and error covariance specifications (that all are uncertain estimation settings).

Ongoing research aiming to diagnose and alleviate numerical diffusion (e.g. Hill et al., 2012) and structural model uncertainty (Forget et al., 2015) is of direct relevance to turbulent transport parameter inversions. Numerical diffusivity of advection schemes or e.g. momentum equation biases could very well contaminate turbulent transport parameter estimates. The fact that the four published inverse estimates all rely on the same dynamical model core could be a serious limitation, but Forget et al. (2015) show that turbulent transport parameter adjustments exceed what may be expected to compensate for model errors due to advection and momentum scheme choices. However, turbulent transport parameter inversions will need to be conducted with a variety of numerical models before one can reach more definitive conclusions in this regard. To start it will be interesting to see how much of the beneficial impacts of the presented $\mathcal{K}_{\mathrm{gm}}$, $\mathcal{K}_{\sigma}$ and $\mathcal{K}_{\mathrm{d}}$ carries over to different ocean and climate models.

Acknowledgements. G. Forget expresses his gratitude to Jean Michel Campin, Patrick Heimbach and Christopher N. Hill for the technical help they provided during the development of ECCO v4. To Carl Wunsch and Ryan Abernathey for useful comments on the presented analysis. To Jane Chapin for useful editorial comments. Efforts of G. Forget and X. Liang were supported in part by National Science Foundation through Grant OCE-0961713 and National Oceanic and Atmospheric Administration through Grant NA10OAR4310135.

References

Abernathey, R., Ferreira, D., and Klocker, A.: Diagnostics of isopycnal mixing in a circumpolar channel, Ocean Model., 72, 1–16, 2013.

Abernathey, R., Marshall, J., Shuckburgh, E., Mazloff, M.: Enhancement of mesoscale eddy stirring at steering levels in the Southern Ocean. J. Phys. Oceanogr., 170?185, 2010.

Abernathey, R. and Marshall, J.: Global surface eddy diffusivities derived from satellite altimetry, J. Geophys. Res.-Oceans, 118, 901–916, 2013.

Abernathey, R., Ferreira, D., and Klocker, A.: Diagnostics of isopycnal mixing in a circumpolar channel, Ocean Model., 72, 1–16, 2013.

Balmaseda, M., Hernandez, F., Storto, A., Palmer, M., Alves, O., Shi, L., Smith, G., Toyoda, T., Valdivieso, M., Barnier, B., Behringer, D., Boyer, T., Chang, Y.-S., Chepurin, G., Ferry, N., Forget, G., Fujii, Y., Good, S., Guinehut, S., Haines, K., Ishikawa, Y., Keeley, S., Kohl, A., Lee, T., Martin, M., Masina, S., Masuda, S., Meyssignac, B., Mogensen, K., Parent, L., Peterson, K., Tang, Y., Yin, Y., Vernieres, G., Wang, X., Waters, J., Wedd, R., Wang, O., Xue, Y., Chevallier, M., Lemieux, J.-F., Dupont, F., Kuragano, T., Kamachi, M., Awaji, T., Caltabiano, A., Wilmer-Becker, K., and Gaillard, F.: The Ocean Reanalyses Intercomparison Project (ORA-IP), Proceedings of the Institute of Marine Engineering, Science, and Technology, J. Operational Oceanogr., 8, s80–s97, doi:10.1080/1755876X.2015.1022329, 2015.

Cole, S. T., Wortham, C., Kunze, E., and Owens, W. B.: Eddy stirring and horizontal diffusivity from Argo float observations: Geographic and depth variability. Geophys. Res. Lett., 42, 3989?3997, doi:10.1002/2015GL063827, 2015

Danabasoglu, G. and Marshall, J.: Effects of vertical variations of thickness diffusivity in an ocean general circulation model, Ocean Model., 18, 122–141, 2007.

Danabasoglu, G., Yeager, S. G., Bailey, D., Behrens, E., Bentsen, M., Bi, D., Biastoch, A., Böning, C., Bozec, A., Canuto, V. M., Cassou, C., Chassignet, E., Coward, A. C., Danilov, S., Diansky, N., Drange, H., Farneti, R., Fernandez, E., Fogli, P. G., Forget, G., Fujii, Y., Griffies, S. M., Gusev, A., Heimbach, P., Howard, A., Jung, T., Kelley, M., Large, W. G., Leboissetier, A., Lu, J., Madec, G., Marsland, S. J., Masina, S., Navarra, A., Nurser, A. G., Pirani, A., Salas y Mélia, D., Samuels, B. L., Scheinert, M., Sidorenko, D., Treguier, A.-M., Tsujino, H., Uotila, P., Valcke, S., Voldoire, A., and Wang, Q.: North Atlantic simulations in Coordinated Ocean-ice Reference Experiments phase {II} (CORE-II). Part I: Mean states, Ocean Model., 73, 76–107, doi:10.1016/j.ocemod.2013.10.005, 2014.

Duffy, P., Eby, M., and Weaver, A.: Effects of sinking of salt rejected during formation of sea ice on results of an ocean–atmosphere–sea ice climate model, Geophys. Res. Lett., 26, 1739–1742, 1999.

Dutkiewicz, S., Sokolov, A. P., Scott, J., and Stone, P. H.: A three-dimensional ocean-seaice-carbon cycle model and its coupling to a two-dimensional atmospheric model: uses in climate change studies, MIT Joint Program on the Science and Policy of Global Change, 2005.

Eden, C.: Thickness diffusivity in the Southern Ocean, Geophys. Res. Lett., 33, L11606 doi:10.1029/2006GL026157, 2006.

Eden, C., Greatbatch, R. J., and Willebrand, J.: A diagnosis of thickness fluxes in an eddy-resolving model, J. Phys. Oceanogr., 37, 727–742, 2007.

Eden, C., Jochum, M., and Danabasoglu, G.: Effects of different closures for thickness diffusivity, Ocean Model., 26, 47–59, 2009.

England, M. H.: Representing the global-scale water masses in ocean general circulation models, J. Phys. Oceanogr., 23, 1523–1552, 1993.

Ferreira, D., Marshall, J., and Heimbach, P.: Estimating eddy stresses by fitting dynamics to observations using a residual-mean ocean circulation model and its adjoint., J. Phys. Oceanogr., 35, 1891–1910, 2005.

Forget, G.: Mapping ocean observations in a dynamical framework: a 2004–06 ocean atlas, J. Phys. Oceanogr., 40, 1201–1221, 2010.

Forget, G. and Ponte, R.: The partition of regional sea level variability, Prog. Oceanogr., ~~, in press,~~ 137, 173–195, doi:10.1016/j.pocean.2015.06.002, 2015.

Forget, G. and Wunsch, C.: Estimated global hydrographic variability, J. Phys. Oceanogr., 37, 1997–2008, 2007.

Forget, G., Ferron, B., and Mercier, H.: Combining Argo profiles with a general circulation model in the North Atlantic. Part 1: Estimation of hydrographic and circulation anomalies from synthetic profiles, over a year, Ocean Model., 20, 1–16, 2008a.

Forget, G., Mercier, H., and Ferron, B.: Combining Argo profiles with a general circulation model in the North Atlantic. Part 2: Realistic transports and improved hydrography, between spring 2002 and spring 2003, Ocean Model., 20, 17–34, 2008b.

Forget, G., Campin, J.-M., Heimbach, P., Hill, C. N., Ponte, R. M, and Wunsch, C.: ECCO version 4: an integrated framework for non-linear inverse modeling and global ocean state estimation, Geosci. Model Dev. Discuss., 8, 3653–3743, doi:10.5194/gmdd-8-3653-2015, 2015.

Fox-Kemper, B., Lumpkin, R., and Bryan, F.: Lateral transport in the ocean interior, in: Ocean Circulation and Climate: a 21st Century Perspective, International Geophysics, Elsevier Science, 185–209, 2013.

Ganachaud, A.: Large-scale mass transports, water mass formation, and diffusivities estimated from World Ocean Circulation Experiment (WOCE) hydrographic data, J. Geophys. Res.-Oceans, 108, 3213, doi:10.1029/2002JC001565, 2003.

Garcia, H., Locarnini, R., Boyer, T., Antonov, J., Zweng, M., Baranova, O., and Johnson, D.: World Ocean Atlas 2009, vol. 4, Nutrients (Phosphate, Nitrate, Silicate), edited by: Levitus, S., NOAA Atlas NESDIS, 71, 2010.

Gaspar, P., Grégoris, Y., and Lefevre, J.-M.: A simple eddy kinetic energy model for simulations of the oceanic vertical mixing: tests at Station Papa and long-term upper ocean study site, J. Geophys. Res., 95, 16179–16193, 1990.

Gent, P. and Mcwilliams, J.: Isopycnal mixing in ocean circulation models, J. Phys. Oceanogr., 20, 150–155, 1990.

Gnanadesikan, A., Abernathey, R., and Pradal, M.-A.: Exploring the isopycnal mixing and helium-heat paradoxes in a suite of Earth System Models, Ocean Sci. Discuss., 11, 2533–2567, doi:10.5194/osd-11-2533-2014, 2014.

Green, J. S.: Transfer properties of the large-scale eddies and the general circulation of the atmosphere. Quart. J. Roy. Meteor. Soc., 96, 157–185, 1970

Griffies, S. M., Adcroft, A. J., Banks, H., Boning, C. W., Chassignet, E. P., Danabasoglu, G., Danilov, S., Deelersnijder, E., Drange, H., England, M., Fox-Kemper, B., Gerdes, R., Gnanadesikan, A., Greatbatch, R. J., Hallberge, R. W., Hanert, E., Harrison, M. J., Legg, S., Little, C. M., Madec, G., Marsland, S. J., Nikurashin, M., Pirani, A., Simmons, H. L., Schroter, J., Samuels, B. L., Treguier, A.-M., Toggweiler, J. R., Tsujino, H., Vallis, G. K., and White, L.: Problems and prospects in large-scale ocean circulation models, in: OceanObs' 09 Conference: Sustained Ocean Observations and Information for Society, Venice, Italy, 21–25 September 2009, 2, 1–24, 2010.

Hill, C., Ferreira, D., Campin, J.-M., Marshall, J., Abernathey, R., and Barrier, N.: Controlling spurious diapycnal mixing in eddy-resolving height-coordinate ocean models – insights from virtual deliberate tracer release experiments, Ocean Model., 45, 14–26, 2012.

Iselin, C.: The influence of vertical and lateral turbulence on the characteristics of the waters at mid-depths, EOS T. Am. Geophys. Un., 20, 414–417, 1939.

Iselin, C. O.: A study of the circulation of the western North Atlantic, Massachusetts Institute of Technology and Woods Hole Oceanographic Institution, Cambridge, Massachusetts, 1936.

Jochum, M., Briegleb, B. P., Danabasoglu, G., Large, W. G., Norton, N. J., Jayne, S. R., Alford, M. H., and Bryan, F. O.: The impact of oceanic near-inertial waves on climate, J. Climate, 26, 2833–2844, 2013.

Karsten, R. H. and Marshall, J.: Constructing the residual circulation of the ACC from observations, J. Phys. Oceanogr., 32, 3315–3327, 2002.

Key, R. M., Kozyr, A., Sabine, C. L., Lee, K., Wanninkhof, R., Bullister, J. L., Feely, R. A., Millero, F. J., Mordy, C., and Peng, T.-H.: A global ocean carbon climatology: results from Global Data Analysis Project (GLODAP), Global Biogeochem. Cy., 18, GB4031, doi:10.1029/2004GB002247, 2004.

Krauß, W., and Böning, C. W.: Lagrangian properties of eddy fields in the northern North Atlantic as deduced from satellite-tracked buoys, J. Mar. Res., 45, 259–291, 1987.
Ledwell, J., Montgomery, E., Polzin, K., Laurent, L. S., Schmitt, R., and Toole, J.: Evidence for enhanced mixing over rough topography in the abyssal ocean, Nature, 403, 179–182, 2000.
Ledwell, J. R., Watson, A. J., and Law, C. S.: Evidence for slow mixing across the pycnocline from an open-ocean tracer-release experiment, Nature, 364, 701–703, 1993.
Ledwell, J. R., Watson, A. J., and Law, C. S.: Mixing of a tracer in the pycnocline, J. Geophys. Res.-Oceans, 103, 21499–21529, 1998.
Liu, C., Köhl, A., and Stammer, D.: Adjoint-based estimation of eddy-induced tracer mixing parameters in the global ocean, J. Phys. Oceanogr., 42, 1186–1206, 2012.
Lumpkin, R. and Speer, K.: Global ocean meridional overturning, J. Phys. Oceanogr., 37, 2550–2562, 2007.
Luyten, J., Pedlosky, J., and Stommel, H.: The ventilated thermocline, J. Phys. Oceanogr., 13, 292–309, 1983.
MacKinnon, J. and Winters, K.: Subtropical catastrophe: significant loss of low-mode tidal energy at 28.9, Geophys. Res. Lett., 32, L15605, doi:10.1029/2005GL023376, 2005.
MacKinnon, J., St Laurent, L., and Naveira Garabato, C.: Diapycnal mixing processes in the ocean interior, in: Ocean Circulation and Climate: a 21st Century Perspective, International Geophysics, Elsevier Science, 159–184, 2013.
Marshall, J., Shuckburgh, E., Jones, H., and Hill, C.: Estimates and implications of surface eddy diffusivity in the Southern Ocean derived from tracer transport, J. Phys. Oceanogr., 36, 1806–1821, 2006.
McDougall, T. J.: The relative roles of diapycnal and isopycnal mixing on subsurface water mass conversion, J. Phys. Oceanogr., 14, 1577–1589, 1984.
Melet, A., Hallberg, R., Legg, S., and Nikurashin, M.: Sensitivity of the ocean state to lee wave–driven mixing, J. Phys. Oceanogr., 44, 900–921, 2014.
Moum, J., Lien, R.-C., Perlin, A., Nash, J., Gregg, M., and Wiles, P.: Sea surface cooling at the equator by subsurface mixing in tropical instability waves, Nat. Geosci., 2, 761–765, 2009.
Munk, W. and Wunsch, C.: Abyssal recipes II: energetics of tidal and wind mixing, Deep-Sea Res. Pt. I, 45, 1977–2010, 1998.
Munk, W. H.: Abyssal recipes, in: Deep Sea Research and Oceanographic Abstracts, vol. 13, Elsevier, 707–730, 1966.

Naveira Garabato, A. C., Polzin, K. L., King, B. A., Heywood, K. J., and Visbeck, M.: Widespread intense turbulent mixing in the Southern Ocean, Science, 303, 210–213, 2004.

Ferrari, R. and Nikurashin, M.: Suppression of eddy diffusivity across jets in the Southern Ocean. J. Phys. Oceanogr., 40, 1501–1519, 2010.

Olbers, D., Wenzel, M., and Willebrand, J.: The inference of North Atlantic circulation patterns from climatological hydrographic data, Rev. Geophys., 23, 313–356, 1985.

Polzin, K., Toole, J., Ledwell, J., and Schmitt, R.: Spatial variability of turbulent mixing in the abyssal ocean, Science, 276, 93–96, 1997.

Ponte, R. M.: An assessment of deep steric height variability over the global ocean, Geophys. Res. Lett., 39, L04601, doi:10.1029/2011GL050681, 2012.

Redi, M. H.: Oceanic isopycnal mixing by coordinate rotation, J. Phys. Oceanogr., 12, 1154–1158, 1982.

Roemmich, D., Boebel, O., Desaubies, Y., Freeland, H., King, B., LeTraon, P.-Y., Molinari, R., Owens, B., Riser, S., Send, U., Kensuke, T., and Wijffels, S.: ARGO: the Global Array of Profiling Floats, CLIVAR Exchanges, 13, 4–5, 1999.

Roemmich, D., Johnson, G. C., Riser, S., Davis, R., Gilson, J., Owens, W. B., Garzoli, S. L., Schmid, C., and Ignaszewski, M.: The Argo Program: observing the global ocean with profiling floats, 2009.

Samelson, R. and Vallis, G. K.: Large-scale circulation with small diapycnal diffusion: the two-thermocline limit, J. Mar. Res., 55, 223–275, 1997.

Schott, F. and Zantopp, R.: On the effect of vertical mixing on the determination of absolute currents by the beta spiral method, Deep-Sea Res., 27, 173–180, 1980.

Siedler, G., Griffies, S., Gould, J., and Church, J.: Ocean Circulation and Climate: a 21st Century Perspective, International Geophysics, Elsevier Science, 2013.

Sloyan, B. M.: Spatial variability of mixing in the Southern Ocean, Geophys. Res. Lett., 32, L18603, doi:10.1029/2005GL023568, 2005.

Speer, K. and Forget, G.: Global distribution and formation of mode waters, in: Ocean Circulation and Climate: a 21st Century Perspective, International Geophysics, Elsevier Science, 211–226, doi:10.1016/B978-0-12-391851-2.00009-X, 2013.

Stammer, D.: Adjusting internal model errors through ocean state estimation, J. Phys. Oceanogr., 35, 1143–1153, 2005.

Toggweiler, J. and Samuels, B.: On the ocean's large-scale circulation near the limit of no vertical mixing, J. Phys. Oceanogr., 28, 1832–1852, 1998.

Tomczak, M. and Large, D. G.: Optimum multiparameter analysis of mixing in the thermocline of the eastern Indian Ocean, J. Geophys. Res.-Oceans, 94, 16141–16149, 1989.
Tulloch, R., Marshall, J., and Smith, K. S.: Interpretation of the propagation of surface altimetric observations in terms of planetary waves and geostrophic turbulence, J. Geophys. Res.-Oceans, 114, C02005, doi:10.1029/2008JC005055, 2009.
Tziperman, E.: On the role of interior mixing and air–sea fluxes in determining the stratification and circulation of the oceans, J. Phys. Oceanogr., 16, 680–693, 1986.
Vallis, G. K.: Atmospheric and Oceanic Fluid Dynamics: Fundamentals and Large-Scale Circulation, Cambridge University Press, Cambridge, UK, 2006.
Walin, G.: On the relation between sea-surface heat flow and thermal circulation in the ocean, Tellus, 34, 187–195, 1982.
Waterhouse, A. F., MacKinnon, J. A., Nash, J. D., Alford, M. H., Kunze, E., Simmons, H. L., Polzin, K. L., St. Laurent, L. C., Sun, O. M., Pinkel, R., Talley, L. D., Whalen, C. B., Huussen, T. N., Carter, G. S., Fer, I., Waterman, S., Naveira Garabato, A. C., Sanford, T. B., and Lee, C. M.: Global patterns of diapycnal mixing from measurements of the turbulent dissipation rate, J. Phys. Oceanogr., 44, 1854–1872, 2014.
Webb, D. and Suginohara, N.: Oceanography: vertical mixing in the ocean, Nature, 409, 37–37, 2001.
Whalen, C., Talley, L., and MacKinnon, J.: Spatial and temporal variability of global ocean mixing inferred from Argo profiles, Geophys. Res. Lett., 39, L18612, doi:10.1029/2012GL053196, 2012.
Wu, L., Jing, Z., Riser, S., and Visbeck, M.: Seasonal and spatial variations of Southern Ocean diapycnal mixing from Argo profiling floats, Nat. Geosci., 4, 363–366, 2011.
Wunsch, C. and Heimbach, P.: Dynamically and kinematically consistent global ocean circulation and ice state estimates, in: Ocean Circulation and Climate: a 21st Century Perspective, International Geophysics, Elsevier Science, 553–579, 2013.
Wyrtki, K.: The oxygen minima in relation to ocean circulation, in: Deep Sea Research and Oceanographic Abstracts, vol. 9, Elsevier, 11–23, 1962.
Zika, J. D., Sloyan, B. M., and McDougall, T. J.: Diagnosing the Southern Ocean overturning from tracer fields, J. Phys. Oceanogr., 39, 2926–2940, 2009.

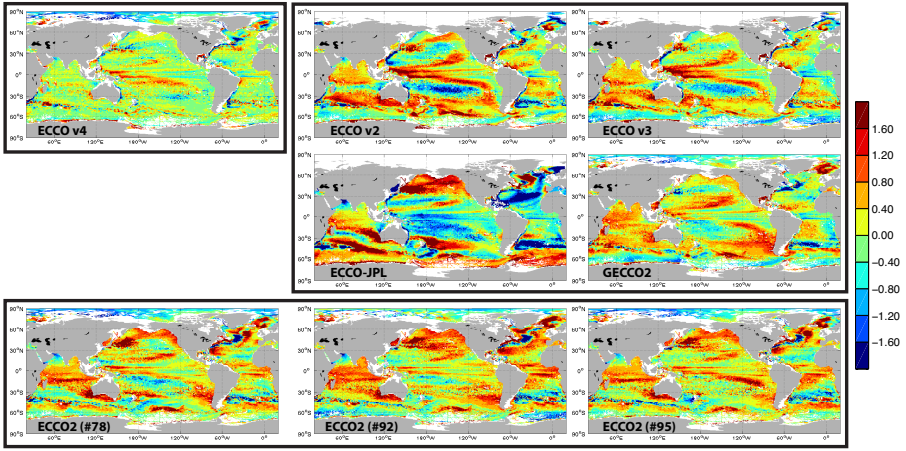

Figure 1. Model-data misfits for temperature at 300 m depth (color scale in °C). The ECCO v4 state estimate (Forget et al., 2015) used in this study is shown in the top left panel. The four panels in the top-right corner show earlier ECCO state estimates that use comparably coarse resolution grids (typically 1° as in ECCO v4). The ECCO v2, ECCO v3, and ~~different adjusted~~ GECCO2 forcing fields were optimized using the adjoint method, ~~but without optimizing~~ whereas ECCO-JPL used a Kalman smoother instead. Unlike ECCO v4, these solutions use un-optimized turbulent transport parameters. The bottom three panels show ECCO2 eddying model solutions (with $\approx 1/6°$ resolution) that use ~~various~~ different sets of forcing fields. Further details on the solutions and these misfits can be found in Forget et al. (2015).

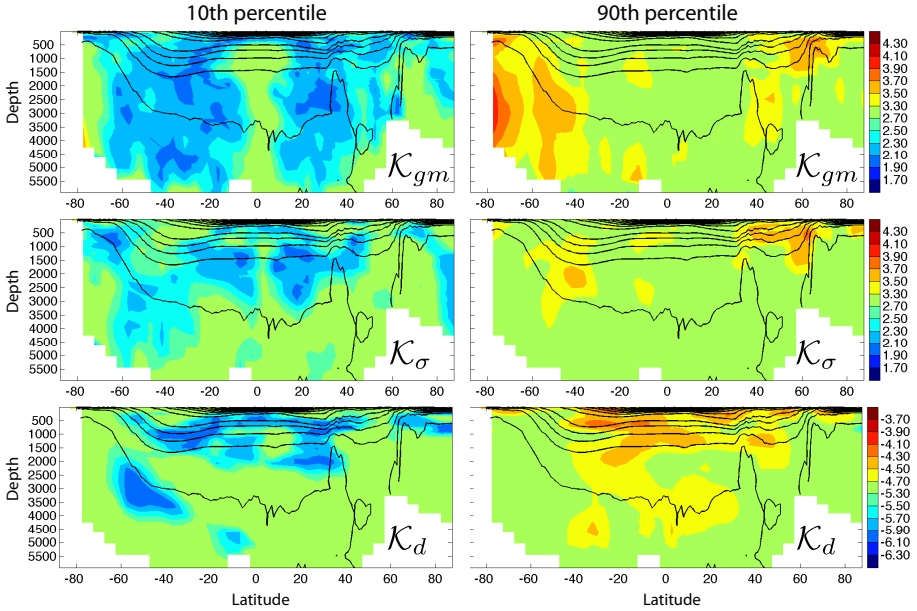

Figure 2. Estimated bolus velocity coefficient (top; $\mathcal{K}_{\mathrm{gm}}$), isopycnal diffusivity (middle; $\mathcal{K}_{\sigma}$) and diapycnal diffusivity (bottom; $\mathcal{K}_{\mathrm{d}}$) in $\mathrm{m}^2\,\mathrm{s}^{-1}$ ($\log_{10}$ color scale). Left: 10th percentile at each latitude and depth; right: 90th percentile. Overlaid black contours denote the time mean zonal mean potential density from the OCCA atlas (Forget, 2010).

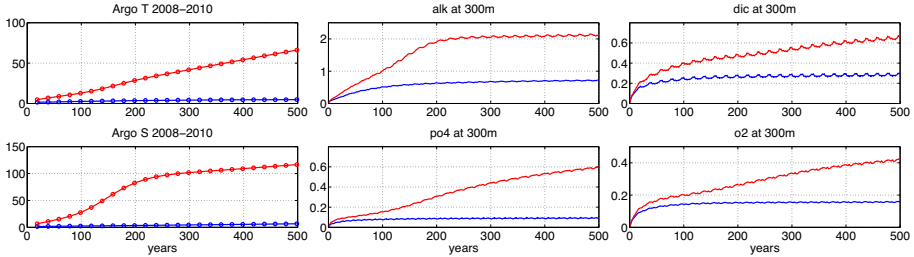

Figure 3. Long term model drifts away from the observed state gauged by repeated comparison with Argo profiles collected over 2008–2010 (top left: T; bottom left: S) and independent climatological data for ~~bio-geochemistry~~ biogeochemistry (middle and right panels) in simulations with (blue) the $\mathcal{K}_{\mathrm{gm}}$, $\mathcal{K}_{\sigma}$ and $\mathcal{K}_{\mathrm{d}}$ estimated parameter maps or (red) the K_{gm}, K_{σ} and K_{d} constant first guess parameters. Each plotted value is a cost function $\overline{d^2/\sigma^2}$ where d is a model–data difference, σ is an uncertainty estimate, and the overbar denotes averaging over all data points. Values of one would indicate model–data differences that are on average exactly at the estimated level of uncertainty. Argo cost function details are reported in Forget et al. (2015). The ~~bio-geochemistry~~ biogeochemistry model is from Dutkiewicz et al. (2005) with settings provided by H. Song (personal communication, 2015). The corresponding cost functions compare annual mean ~~bio-geochemistry~~ biogeochemistry model fields at 300 m with the climatologies that were used to initialize the model. The 300 m climatology standard deviation is further used as an ad-hoc uncertainty estimate to form a cost function. Top middle: alkalinity (Key et al., 2004); bottom middle: phosphate (Garcia et al., 2010); top right: dissolved inorganic carbon (Key et al., 2004); bottom right: dissolved oxygen (Garcia et al., 2010).

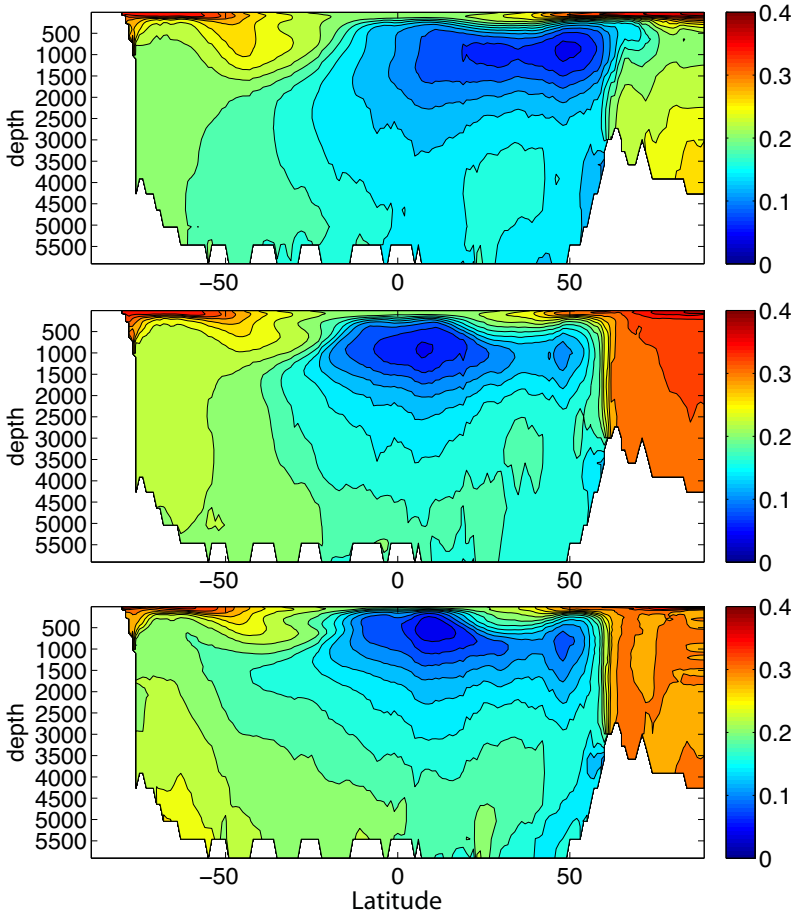

Figure 4. Zonal mean oxygen concentration (in $\mathrm{mol\,m^{-3}}$) from Garcia et al. (2010) (bottom panel) and from the two 500 years simulations (see Fig. 3 caption for details) using the $\cancel{K_{gm}}\underset{\sim}{K_{gm}}$, $\cancel{K_{\sigma}}\underset{\sim}{K_{\sigma}}$, $\cancel{K_{d}}\underset{\sim}{K_{d}}$ estimate (middle) or the $\cancel{K_{gm}}K_{gm}$, $\cancel{K_{\sigma}}K_{\sigma}$, $\cancel{K_{d}}K_{d}$ first guess (top).

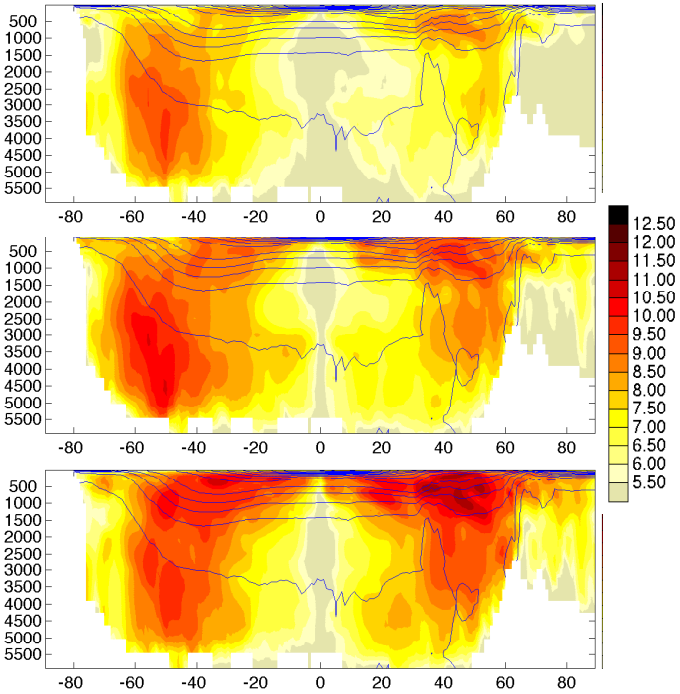
500
1000
1500
2000
2500
3000
3500
4000
4500
5000
5500
-80
-60
-40
-20
0
20
40
60
80
12.50
12.00
11.50
11.00
10.50
10.00
9.50
9.00
8.50
8.00
7.50
7.00
6.50
6.00
5.50

Figure 5. Sensitivity to $\mathcal{K}_{\text{gm}}$ associated with 1992-2001 altimetry (top), 1992-2011 altimetry (middle), and Argo T and S profiles (bottom). More than 98% of Argo profiles were collected after 2001. In each case, the squared model-data distance J is selected accordingly, and $\frac{\partial J}{\partial K_{\text{gm}}}$ is computed with the adjoint model. The adjoint model and J_{Argo} are documented in details in Forget et al. (2015) . For altimetry, J uses the large-scale formulation of Forget and Ponte (2015) . In all cases, turbulent optimization parameters are reset to their unadjusted values, so that the adjoint computation is representative of the starting point of the estimation process. The results are displayed non-dimensionally as $log_{10}(||u_{\text{gm}} \frac{\partial J}{\partial K_{\text{gm}}}||^2)$ where $||.||^2$ denotes the zonal mean squared norm, and $u_{\text{gm}} = 500$ $\text{m}^2\,\text{s}^{-1}$.

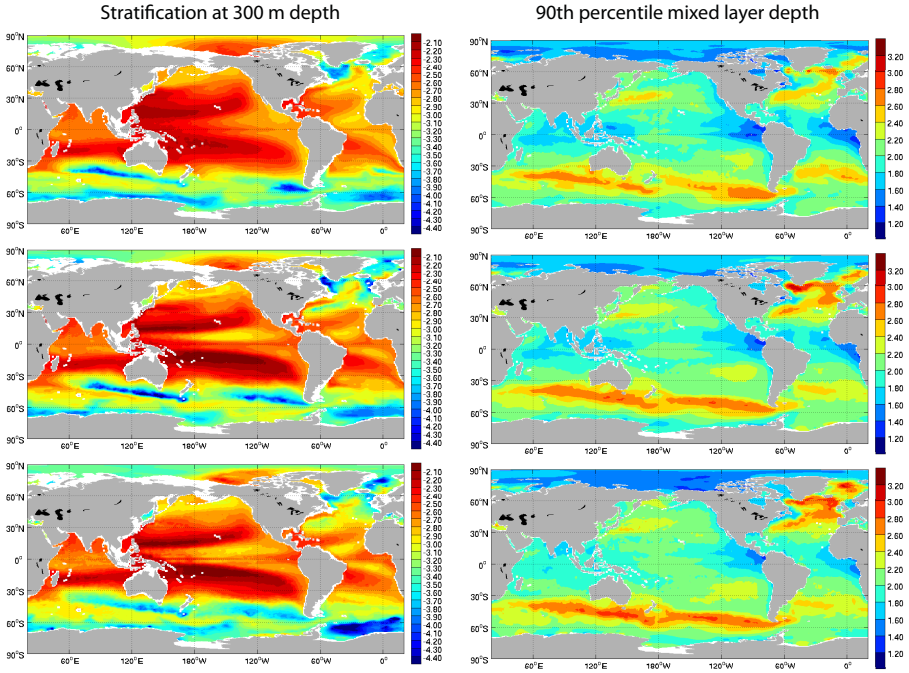

Figure 6. (Left) median stratification at 300 m depth (shown as $\log_{10}(\frac{\partial \rho}{\partial z})$ in kg m^{-4}) and (right) 90 percentile mixed layer depth (shown as $\log_{10}$(mld) in m) for (bottom) in situ profiles, (middle) the corresponding state estimate profiles, and (top) model profiles generated by resetting $\mathcal{K}_{\mathrm{gm}}$, $\mathcal{K}_{\sigma}$, $\mathcal{K}_{\mathrm{d}}$ to the K_{gm}, K_{σ}, K_{d} first guess while retaining all other settings of the state estimate. Percentiles are computed from the distribution of individual profile values within grid boxes and mapped.

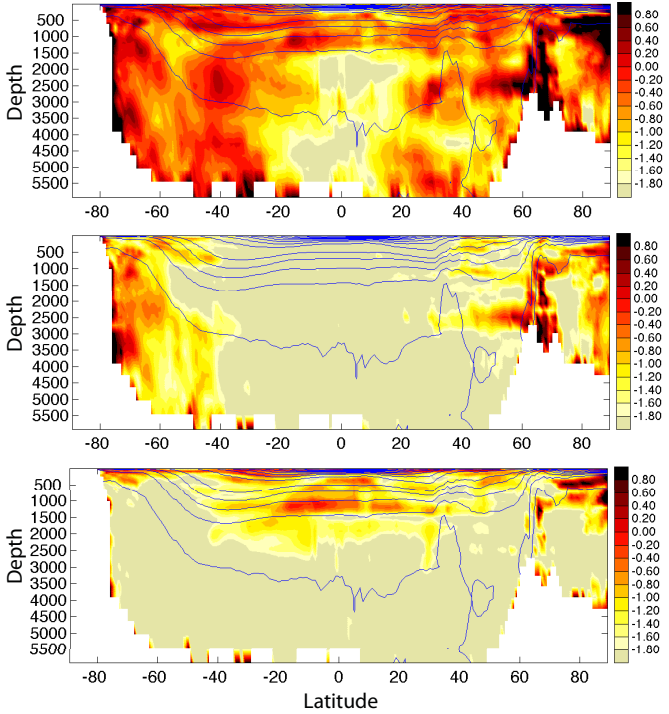

Figure 7. Sensitivity of ocean stratification to $\mathcal{K}_{\text{gm}}$ (top), $\mathcal{K}_\sigma$ (middle), and $\mathcal{K}_{\text{d}}$ (bottom). Mean squared deviations are computed between perturbation experiments and the state estimate for the 2008–2010 monthly climatology of $\frac{\partial \rho}{\partial z}$, and then normalized by the corresponding state estimate variance. The color shading shows the $\log_{10}$ of this ratio. Thus, orange denotes $> 10\,\%$ differences, while dark red denotes $> 100\,\%$ differences. The perturbation experiment where the $\mathcal{K}_{\text{gm}}$ (resp. $\mathcal{K}_\sigma$, $\mathcal{K}_{\text{d}}$) estimate is reset to the constant K_σ (resp. K_σ, K_{d}) first guess is shown at the top (resp. middle, bottom). Overlaid contours: zonal mean potential density from the OCCA atlas.

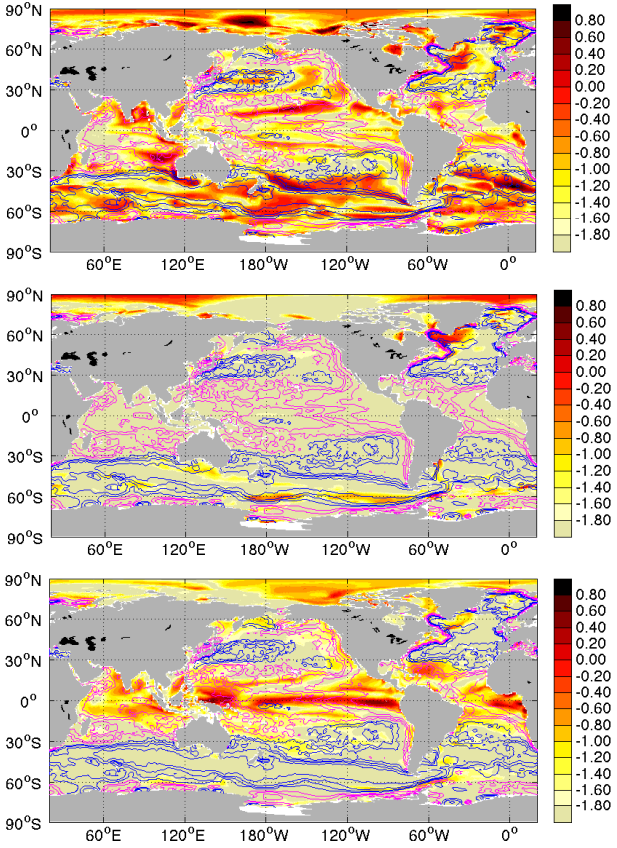

Figure 8. Mixed layer depth sensitivity (color shading) to $\mathcal{K}_{\text{gm}}$ (top), $\mathcal{K}_\sigma$ (middle), and $\mathcal{K}_{\text{d}}$ (bottom). Computational and plotting details are similar to Fig. 7. Overlaid blue contours (resp. magenta contours) denote the 60, 70, 80, 90th (resp. 10, 20, 30, 40th) percentiles of the observed mixed layer depth map (mld(x, y) from the bottom right panel of Fig. 6).

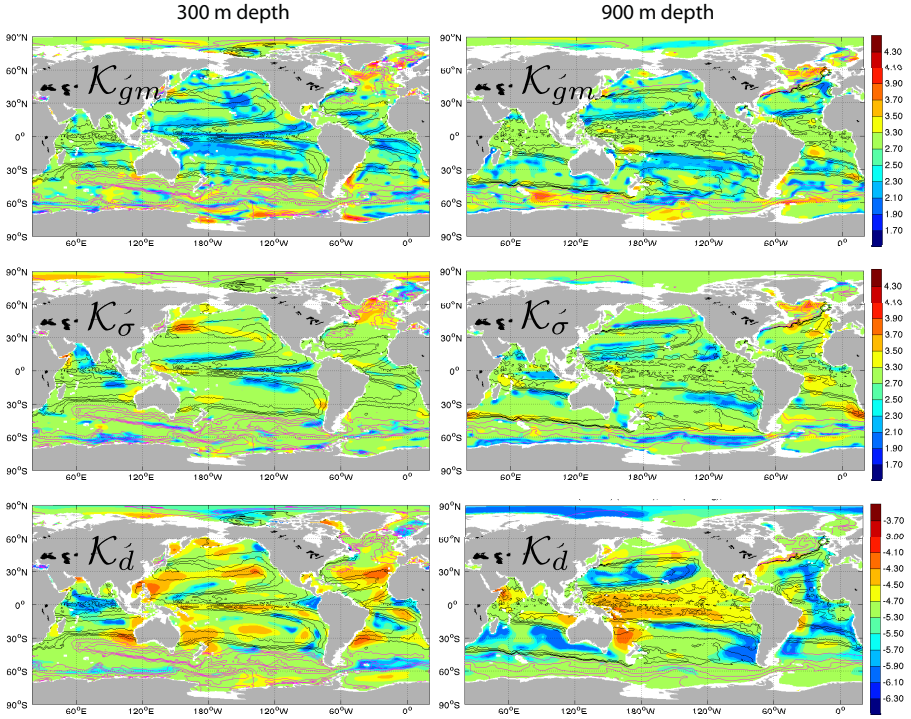

Figure 9. Estimated bolus velocity coefficient (top), isopycnal diffusivity (middle) and diapycnal diffusivity (bottom) at 300 m depth (left) and 900 m depth (right) in $m^2\,s^{-1}$ ($\log_{10}$ color scale). The respective first guess values are 10^3, 10^3 and 10^{-5} $m^2\,s^{-1}$. Each overlaid contour corresponds to a percentile of the observed stratification map $\frac{\partial \rho}{\partial z}(x,y)$ that is depicted 300 m in Fig. 6 (bottom left)~~for the 300depth case~~. Black contours (resp. magenta contours) denote the 60th, 70th, 80th, 90th (resp. 10th, 20th, 30th, 40th) percentiles of $\frac{\partial \rho}{\partial z}(x,y)$.

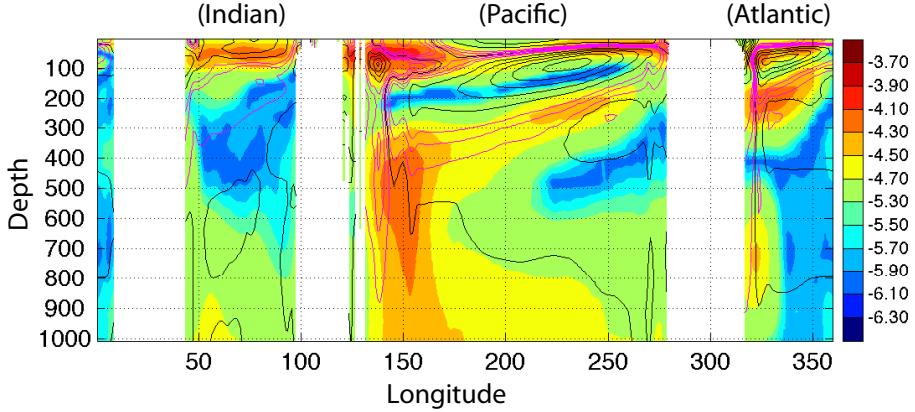

Figure 10. Estimated diapycnal diffusivity ($\mathcal{K}_d$) at the equator in $m^2\,s^{-1}$ ($\log_{10}$ color scale). Black and magenta contours denote the time mean zonal velocity from the state estimate. Black contours are separated by $10\,cm\,s^{-1}$ whereas magenta contours are separated by $4\,cm\,s^{-1}$ in the range within $\pm 10\,cm\,s^{-1}$.

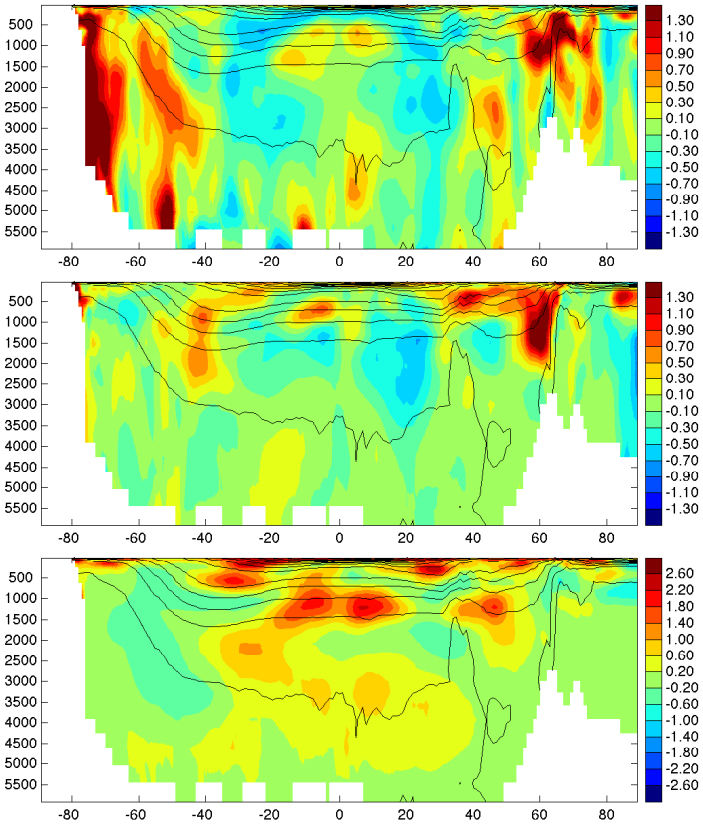

Figure 11. Zonal mean ~~bolus velocity coefficient adjustment~~ of $\frac{\mathcal{K}_{gm}-K_{gm}}{K_{gm}}$ ($\mathcal{K}_{gm}$ ~~— 1000~~top)~~in~~ , $\frac{\mathcal{K}_\sigma-K_\sigma}{K_\sigma}$ (middle), and $\frac{\mathcal{K}_d-K_d}{K_d}$ (bottom) with $K_{gm}=10^3$, $K_\sigma=10^3$ and $K_d=10^{-5}$ $m^2\,s^{-1}$~~color scale~~. Overlaid contours: zonal mean potential density from the OCCA atlas.

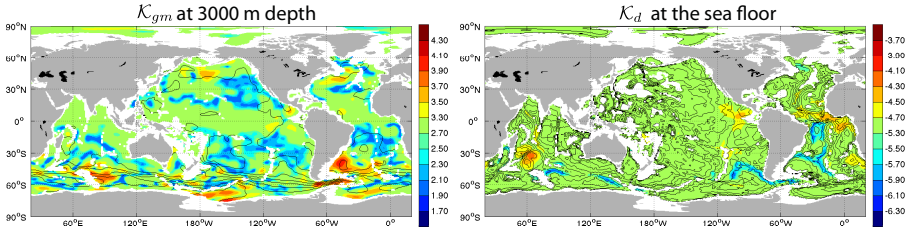

Figure 12. Estimated bolus velocity coefficient at 3000 m depth (left) and diapycnal diffusivity immediately above the sea floor (right) in $m^2\,s^{-1}$ ($\log_{10}$ color scale). Overlaid contours: σ_1 potential density from the OCCA atlas in 0.02 $kg\,m^{-3}$ increments (left) and ocean depth in 500 m increments (right).

Manuscript prepared for Ocean Sci. Discuss.
with version 2014/09/16 7.15 Copernicus papers of the LaTeX class copernicus.cls.
Date: 19 September 2015

On the observability of turbulent transport rates by Argo: supporting evidence from an inversion experiment

G. Forget[1], D. Ferreira[2], and X. Liang[1]

[1]Dept. of Earth, Atmospheric and Planetary Sciences, Massachusetts Institute of Technology, Cambridge, MA 02139, USA
[2]Department of Meteorology, University of Reading, Reading, UK

Correspondence to: G. Forget (gforget@mit.edu)

Discussion Paper | Discussion Paper | Discussion Paper | Discussion Paper |

Abstract

Although estimation of turbulent transport parameters using inverse methods is not new, there is little evaluation of the method in the literature. Here, it is shown that extended observation of the broad-scale hydrography by Argo provides a path to improved estimates of regional turbulent transport rates. Results from a 20 year ocean state estimate produced with the ECCO v4 non-linear inverse modeling framework provide supporting evidence. Turbulent transport parameter maps are estimated under the constraints of fitting the extensive collection of Argo profiles collected through 2011. The adjusted parameters dramatically reduce misfits to in situ profiles as compared with earlier ECCO solutions. They also yield a clear reduction in the model drift away from observations over multi-century long simulations, both for assimilated variables (temperature and salinity) and independent variables (biogeochemical tracers). Despite the minimal constraints imposed specifically on the estimated parameters, their geography is physically plausible and exhibits close connections with the upper ocean ocean stratification as observed by Argo. The estimated parameter adjustments furthermore have first order impacts on upper-ocean stratification and mixed layer depths over 20 years. These results identify the constraint of fitting Argo profiles as an effective observational basis for regional turbulent transport rates inversion. Uncertainties and further improvements of the method are discussed.

1 Introduction

Direct observational estimates of vertical and lateral turbulent transport rates are largely limited to studies of surface drifter dispersion (e.g. Krauß and Böning, 1987), surface eddy fluxes estimated from satellite data (e.g. Abernathey and Marshall, 2013), occasionally released tracer dispersion (e.g. Ledwell et al., 1993), and rare micro-structure measurements (see Waterhouse et al., 2014). However the vast collection of in situ profiles provided by Argo (Roemmich et al., 1999, 2009) may offer new opportunities to infer turbulent transport rates from the sea surface to 2000 m depth. Inferences of diffusivities is possible through

the analysis of Argo variance fields combined with conceptual turbulence models (Wu et al., 2011; Whalen et al., 2012; Cole et al., 2015). The extensive observation of the broad-scale hydrography characteristics by Argo may also provide a basis for the inversion of turbulent transport rates.

The idea that turbulent transports can be inferred from observed characteristics of the broad-scale hydrography goes back to Iselin (1936, 1939) and likely even further. It is for example the basis of the Munk (1966) estimate of diapycnal diffusivity from temperature profile curvatures below 1000 m (following upon Wyrtki, 1962). Many subsequent studies have pursued comparable inferences of turbulent transport rates (or parameters) from observed broad-scale hydrography characteristics using conceptual models as well as general circulation models and adjoint techniques (e.g. Schott and Zantopp, 1980; Walin, 1982; McDougall, 1984; Olbers et al., 1985; Tziperman, 1986; Tomczak and Large, 1989; Ganachaud, 2003; Stammer, 2005; Ferreira et al., 2005; Lumpkin and Speer, 2007; Zika et al., 2009; Liu et al., 2012). The large influence of vertical and lateral turbulence in setting the large-scale characteristics of the ocean state in numerical models (e.g. Danabasoglu and Marshall, 2007; Eden et al., 2009; Griffies et al., 2010; Jochum et al., 2013; Gnanadesikan et al., 2014; Melet et al., 2014) underscores that the large-scale ocean state observation carries a wealth of information on turbulent transport rates.

Despite this long history and strong modeling evidence, it is not clear that inverse parameter estimates are useful, robust and/or physically meaningful. Munk's estimate of diapycnal diffusivity provides an example of the possible downfall of the method (Munk 1966; see also Munk and Wunsch 1998). Munk's estimate of about $10^{-4}\,\mathrm{m\,s^{-1}}$ that was originally based upon a one-dimensional model of the Pacific led to the search for the "missing mixing" since direct observations of diapycnal mixing in the thermocline were an order of magnitude smaller than Munk's value (Ledwell et al., 1998, 2000). However it is now commonly accepted that neglected physics (e.g. the adiabatic upwelling of North Atlantic Deep Water in the Southern Ocean; Toggweiler and Samuels 1998, Webb and Suginohara 2001) could explain the discrepancy.

Importantly, this example illustrates the difficulty in interpreting inverse parameter estimates, and the possible confusion brought on by assumptions built in the fitted model. In light of the well documented heterogeneity in ocean mixing rates and processes (reviewed in MacKinnon et al., 2013; Fox-Kemper et al., 2013) the notion that ocean mixing as a whole can be cast into a one-dimensional model now seems incongruous. Models of extreme simplification, while they can illuminate individual mechanisms, also discount the composite and complex essence of ocean observations.

General circulation models used within a least-squares framework a priori provide a suitable framework to avoid mis-interpreting observations (e.g. aliased small-scale signals) while taking advantage of complementary data sets (e.g. altimetry) and constraints (e.g. atmospheric re-analyses) to infer large-scale ocean balances and diagnose ocean variability (see Wunsch and Heimbach, 2013, for a review). However the few publications that followed this approach to infer turbulent transport parameters (Stammer, 2005; Ferreira et al., 2005; Liu et al., 2012) provide little, if any, evaluation of the method and its results. At best, they point to the usefulness of the estimated parameters in an ad-hoc manner – for example Ferreira et al. (2005) derived a parameterization of eddy diffusivity as a function of stratification that improved the un-constrained ocean model solution.

How many and which degrees of freedom may be well constrained by available observations is just one of the rather technical, yet crucial questions that have never been tackled. Thus one could still argue that parameter inversion (along with forcing fields adjustment) through general circulation models is nothing more than an objective and practical way of tuning these models (i.e. a marginally useful approach). Whether the estimated parameters have any intrinsic value beyond the chosen estimation framework and settings (assimilated observations, period of assimilation, numerical model, etc.) remains unclear just as in the case of conceptual models. Further assessment of data constraints and parameter estimates is clearly needed and equally justified given the obvious importance of the subject matter.

In this paper we aim to demonstrate that extended observation of the broad-scale hydrography by Argo (see, e.g. Forget and Wunsch, 2007; Forget, 2010; Speer and Forget,

2013) should translate into improved estimates of upper ocean turbulent transport rates. In other words, we seek to assert that turbulent transport rates are "observable" by means of Argo's collection of temperature and salinity profiles. This is clearly not a trivial proposition given the variety and heterogeneity of oceanic processes intermingled within observational data – especially in the upper ocean. Overarching oceanographic questions regarding the observability of turbulent transport rates by means of broad-scale measurements largely remain to be answered such as: which specific features of the ocean state are informative of which turbulent transport rates? How precise may inverse estimates of turbulent transport rates be depending on the limited data availability? How are inverse problems best formulated to take full advantage of available observations?

The presented analysis reaches preliminary answers to these open questions, while providing clear supporting evidence that observations of the large-scale ocean stratification by Argo yield useful constraints to estimate turbulent transport parameters, and establishing a frame of reference for further research into their observability. It focuses on the Forget et al. (2015) ocean state estimate over 1992–2011 covering the Argo era and mainly on the 0–2000 m oceanic layer that Argo observes extensively. In this framework, vertical and lateral turbulent transport parameters are estimated by fitting the simulated large-scale ocean state to observations (notably Argo profiles of temperature and salinity). Even though minimal constraints are imposed on the parameters themselves, their geography and impacts are found to be physically meaningful and shown to be useful beyond the estimation procedure.

Section 2 summarizes the estimation method, establishes that the estimated parameters are broadly consistent with the observed large-scale ocean state, and shows that they reduce spurious model drifts using independent biogeochemistry data. Section 3 demonstrates the high sensitivity of the observed upper-ocean stratification to the estimated parameters. This result provides clear supporting evidence that Argo profile collections yield a useful observational constraint of regional turbulent transport rates. The estimated turbulent parameters themselves and their relationship to the large-scale ocean state are dis-

cussed in Sect. 4. Section 5 provides a discussion of the uncertainties in the approach. The findings are summarized and perspectives are drawn in Sect. 6.

2 Reduced model errors

The "Estimating the Circulation and Climate of the Ocean version 4" (ECCO v4) estimate of the evolving ocean state over the period 1992–2011 as well as the associated model and estimation settings are presented in detail in Forget et al. (2015). In summary, the 20 year solution of the global one degree resolution model is fitted to a suite of data constraints, including the vast collection of Argo profiles of temperature (T) and salinity (S), through iterative adjustments of turbulent transport parameters (time-invariant), atmospheric forcing fields (bi-weekly) and initial conditions (on 1992/01/01). Forget et al. (2015) show that the turbulent transport parameter adjustments are particularly important to the close fit of ECCO v4 to observed in situ profiles. They allow a clear reduction in widespread misfits in ECCO v4 (Fig. 1; top left panel) as compared with (1) earlier ECCO solutions that optimized surface forcing fields but not turbulent transport parameters (top right corner panels) and (2) ECCO2 eddying model simulations (bottom three panels).

The turbulent transport parameters being estimated, and the focus of this paper, are time-invariant three dimensional maps of bolus velocity coefficient $\mathcal{K}_{\mathsf{gm}}$ (Gent and Mcwilliams, 1990), isopycnal diffusivity $\mathcal{K}_\sigma$ (Redi, 1982), and background diapycnal diffusivity $\mathcal{K}_{\mathsf{d}}$ (aside from mixed layer parameterizations). The tendency equation for a tracer ϕ in the ocean interior can thus be written in simplified form as:

$$\frac{\partial \phi}{\partial t} + \nabla \cdot (\boldsymbol{u}\,\phi + \boldsymbol{u}^\star\,\phi) = \nabla \cdot (\mathcal{K}_\sigma \nabla_\sigma \phi) + \frac{\partial}{\partial z}\left(\mathcal{K}_z \frac{\partial \phi}{\partial z}\right), \tag{1}$$

where $\mathcal{K}_z$ includes $\mathcal{K}_{\mathsf{d}}$ plus contributions from mixed layer parameterizations (Gaspar et al. 1990, Duffy et al. 1999, plus simple convective adjustment), $\nabla_\sigma \phi$ is the lateral tracer gradient on isopycnal surfaces (Redi, 1982), $\boldsymbol{u}$ is the Eulerian velocity, and $\boldsymbol{u}^\star$ is the parameterized bolus velocity representing the advective (adiabatic) effect of meso-scale eddies. After

Gent and Mcwilliams (1990) the non-divergent bolus velocity is evaluated as $\boldsymbol{u}^\star = -\nabla \times \Psi^\star$ where $\Psi^\star = (\mathcal{K}_{\mathsf{gm}} S_y, \mathcal{K}_{\mathsf{gm}} S_x, 0)$ is the bolus streamfunction, and S_x and S_y are the isopycnal slopes in the zonal and meridional directions, respectively.

The first guess values are the constants $K_{\mathsf{gm}} = 10^3$, $K_\sigma = 10^3$ and $K_{\mathsf{d}} = 10^{-5}\,\mathrm{m^2\,s^{-1}}$ with respective uncertainties set to $u_{\mathsf{gm}} = 500$, $u_\sigma = 500$ and $u_{\mathsf{d}} = 10^{-4}\ \mathrm{m^2\,s^{-1}}$. As part of ECCO v4, the specification of error covariances for $\mathcal{K}_{\mathsf{gm}}$, $\mathcal{K}_\sigma$ and $\mathcal{K}_{\mathsf{d}}$ is limited to imposing smoothness at the scale of three grid points, thus allowing regional adjustments to emerge simply from observational constraints under the dynamical model constraint. The respective ranges of permitted adjustment are $10^2 < \mathcal{K}_{\mathsf{gm}} < 10^4$, $10^2 < \mathcal{K}_\sigma < 10^4$, and $10^{-6} < \mathcal{K}_{\mathsf{d}} < 5 \times 10^{-4}\,\mathrm{m^2\,s^{-1}}$. The specified ranges span values found (directly or indirectly) in observations as well as values typically used in general circulation models.

Note that the constraints imposed specifically on the turbulent parameters (smoothness and range) are minimal on purpose. One could envision imposing further constraints, for example on the vertical structure or the energetics of the turbulent parameters. Here, instead, the turbulent parameters can adjust freely within the specified ranges that reflect their large a priori uncertainty at the scale of a few grid points. Accordingly, the adjusted parameters spread out over the specified ranges as a result of observational constraints being imposed (Fig. 2). The primary objective of this paper is to reveal the observational basis to these adjustments being provided by the rapidly growing in-situ data base (Sects. 3 and 4).

To test the estimated turbulent parameters beyond the 20 years of the estimation window, two model integrations are carried out for 500 years that perpetually loop over the 1992–2011 forcing of the ECCO v4 state estimate. One integration uses the estimated parameters while the other uses the constant first guess parameters (which, we should underscore, are common values used in ocean models of comparable horizontal resolution). The turbulent transport parameter adjustments yield a clear reduction in the model's tendency to drift away from observations over multiple centuries (Fig. 3). This is true not only for the physical variables that were directly constrained by Argo profiles (left panels) but also for biogeochemical variables that were not (middle and right panels).

The biogeochemistry result is most remarkable as it provides independent evidence that the turbulent transport parameter adjustments as estimated from observations of physical variables reduce internal model error more generally. In itself this novel result demonstrates strong constraints imposed (directly or indirectly) by observations of the physical state on biogeochemistry. The resulting improvement in biogeochemistry (Fig. 3) implies that regional turbulent transport rates are at least partly observable by available observations of physical variables. It further motivates the assessment of the estimated turbulent transport parameters and of their observational basis presented below.

Before returning the focus to the 20 year estimation period, it is worth illuminating the consequences of $\mathcal{K}_{\mathsf{gm}}$, $\mathcal{K}_\sigma$ and $\mathcal{K}_{\mathsf{d}}$ over longer time scales (Fig. 4). The fact that the benefits of the ocean state estimation procedure extends much beyond its 20 years (Fig. 3) and through the abyss over centennial time scales (not shown) is indeed clearly not a trivial result. It implies dramatic changes in the formation and ventilation of oceanic water masses, as demonstrated by zonal mean oxygen concentrations after 500 years (Fig. 4).

The fact that the ECCO v4 turbulent transport parameter adjustments (Fig. 2) increase the simulated oxygen concentration in the subtropical abyss (Fig. 4) in particular denotes an intensification in the formation and spreading of Antarctic Bottom Water (also evident near Antarctica at all depths). The improved maintainance of a high oxygen content in the Arctic and of the mid-latitude oxygen minimum region is equally remarkable (Fig. 4). While the oxygen minimum exists due to oxygen consumption by biogeochemistry, it is also largely shaped by physical processes (Wyrtki, 1962). Fig. 4 provides evidence that it is effectively constrained by Argo's collection of T and S profiles via their constraint of turbulent transport parameters revealed in Sects. 3 and 4. Whether the constraint of the oxygen minimum results directly from $\mathcal{K}_{\mathsf{gm}} - K_{\mathsf{gm}}$, $\mathcal{K}_\sigma - K_\sigma$ and $\mathcal{K}_{\mathsf{d}} - K_{\mathsf{d}}$ appearing in the biogeochemical tracer equations or rather indirectly from improvements in other physical variables (T, S, etc.) impacting biochemistry is an interesting question left for further investigation.

3 Parametric controls of ocean stratification

The new constraints on turbulent transport parameter inversions brought by data collected over the past decade can most immediately be gauged using linear adjoint sensitivities (Fig. 5 for $\mathcal{K}_{\mathsf{gm}}$). The results show that the constraint provided by one decade of Argo data collection (bottom) generally exceeds that provided by two decades of altimetry (middle). Furthermore, the large sensitivity increase seen upon moving from the top panel (10 years of altimetry) to the middle panel (20 years of altimetry) illustrates how the second decade of Argo data collection should even further solidify the observational basis to turbulent transport parameter inversions. These considerations motivate the detailed investigation of the existing Argo data constraint presented below.

The geography and values of ocean stratification ($\frac{\partial \rho}{\partial z}$ and mixed layer depths) are a priori particularly relevant to turbulent transport rate inferences. Stratification is indeed a prime candidate amongst observational constraints as it is intimately related to potential vorticity, water mass formation and ventilation, which in turn strongly constrain the general ocean circulation (see e.g. Walin, 1982; Luyten et al., 1983). Argo's collection of T and S profiles yields an extensive observation of ocean stratification (Fig. 6). Its importance as an observational constraint of $\mathcal{K}_{\mathsf{gm}}$, $\mathcal{K}_{\sigma}$ and $\mathcal{K}_{\mathsf{d}}$ is established below.

At 300 m outside of the tropics, lows in $\frac{\partial \rho}{\partial z}$ (Fig. 6, bottom left) delineate regions of deep winter convection (Fig. 6, bottom right) and mode water formation (see Speer and Forget, 2013). In the tropics at 300 m, lows in $\frac{\partial \rho}{\partial z}$ denote thermoclines shallower than 300 m. Conversely, subtropical and tropical thermoclines intersecting 300 m are marked by highs in $\frac{\partial \rho}{\partial z}$ (Fig. 6, bottom left). The state estimate's stratification geography and values (Fig. 6, middle left) generally are in very good agreement with Argo observations (Fig. 6, bottom left). Thus the estimated $\mathcal{K}_{\mathsf{gm}}$, $\mathcal{K}_{\sigma}$ and $\mathcal{K}_{\mathsf{d}}$ are consistent with the observed stratification.

To evaluate the full non-linear sensitivity of ocean stratification to each of the three parameters, three forward perturbation experiments are conducted. In each experiment on parameter is individually reset to its constant first guess value. It is worth recalling that atmospheric forcing field adjustments (in temperature, specific humidity, downward radia-

tion, precipitation, and wind stress) have a lesser impact on the subsurface hydrography than turbulent transport parameter adjustments do in ECCO v4 (Forget et al., 2015). In particular it is readily evident in Fig. 6 that the realism of the state estimate stratification is noticeably improved by the turbulent transport parameter adjustments (compare middle and top panels). Therefore the adjusted atmospheric forcing fields are retained in all perturbation experiments presented here to focus on turbulent transport parameters and their observability.

The mean squared deviation of $\frac{\partial \rho}{\partial z}$ between each perturbed solution and the state estimate over the period 2008–2010, normalized by the corresponding $\frac{\partial \rho}{\partial z}$ variance, is shown in logarithmic scale as a function of latitude and depth (Fig. 7). Logarithmic values above 0 indicate $\frac{\partial \rho}{\partial z}$ contrasts between solutions being as large as the zonal and seasonal mean $\frac{\partial \rho}{\partial z}$ variance in the state estimate. Such large impact of turbulent transport parameter adjustments on $\frac{\partial \rho}{\partial z}$ occurs at all latitudes in the upper 2000 m. Figure 7 thus provides decisive supporting evidence that inversion of regional turbulent transport rates is effectively guided by the constraint of fitting Argo profiles. The collocation of large ocean stratification changes (Fig. 7) and turbulent transport parameter adjustments (Fig. 2) further confirms that they are tied to each other in ECCO v4 (see Sect. 4 for more detail).

Generally in the upper 2000 m and over the whole water column at high latitudes, ocean stratification is found to be more sensitive to $\mathcal{K}_{\mathsf{gm}}$ (Fig. 7, top) than to $\mathcal{K}_\sigma$ (middle) or $\mathcal{K}_{\mathsf{d}}$ (bottom). The predominant impact of $\mathcal{K}_{\mathsf{gm}}$ suggests that ocean stratification profiles may most efficiently constrain (i.e. observe) the rates of bolus advection, albeit with several noteworthy exceptions. High sensitivity to $\mathcal{K}_\sigma$ (Fig. 7, middle) is found at high latitudes. The impact of $\mathcal{K}_\sigma$ on $\frac{\partial \rho}{\partial z}$ is indirect since $\nabla_\sigma \phi$ in Eq. (1) vanishes for $\phi = \sigma$. It does however have dynamical impacts and it is not surprising that they are magnified at high latitudes where dense layers outcrop and interact with mixed layer and sea-ice processes (e.g. see England, 1993; Zika et al., 2009). Furthermore haline density variations overcome thermal density variations at those latitudes (e.g. see Forget and Wunsch, 2007; Forget and Ponte, 2015) and this transition provides an environment conducive to dynamical impacts of $\mathcal{K}_\sigma$. High sensitivity to $\mathcal{K}_{\mathsf{d}}$ is found in the tropics and in the Arctic in the 0–2000 m layer, as well as

near the sea surface at all latitudes. This result implies that observation of the stratification broad-structure informs us of diapycnal diffusion rates in these regions.

Winter mixed layers modulate water mass transformations and the penetration of surface buoyancy fluxes. As such they are a key factor in ocean stratification and deserve special attention. The state estimate closely agrees with the geography and magnitude of observed mixed layers (Fig. 6, right panels). The sensitivity of mixed layer depths to turbulent transport parameters (Fig. 8) varies on a regional basis and mostly reflects the underlying stratification sensitivity (Fig. 7). Logarithmic values above 0 in Fig. 8 indicate that changes in mixed layer depths that result from the parameter adjustments are as large as the seasonal contrasts seen in the state estimate. Such differences in mixed layer depths provide additional evidence of efficient constraints imposed by Argo on turbulent transport rates.

Several dynamical regimes can be distinguished in Figs. 7 and 8 that are in broad agreement with theoretical views and worth commenting upon before proceeding with further assessment of the geography (Sect. 4) and uncertainty (Sect. 5) of $\mathcal{K}_{\mathsf{gm}}$, $\mathcal{K}_\sigma$ and $\mathcal{K}_{\mathsf{d}}$. The thermocline in the upper 2000 m (between 60° S and 60° N) is primarily adjusted through adiabatic circulation controls (Fig. 7, top panel) rather than diapycnal mixing changes (Fig. 7, bottom panel). This behavior is prompted by data constraints leading to $\mathcal{K}_{\mathsf{gm}}$, $\mathcal{K}_\sigma$ and $\mathcal{K}_{\mathsf{d}}$ rather than by a priori assumptions. Thus, Fig. 7 provides objective observational support for predominantly adiabatic, ventilated thermocline theories (see Vallis, 2006).

The sizable impact of the increased $\mathcal{K}_{\mathsf{d}}$ at the base of the ventilated thermocline further supports the notion that it is embedded in an internal thermocline (Samelson and Vallis, 1997) where diffusion balances advection (see Figs. 2 and 7). Another regime appears near the sea surface in the tropics, where shallow mixed layers and stratification also strongly respond to background diapycnal mixing (Figs. 7–8). Finally, high latitudes where deep isopycnals outcrop and experience large isopycnal variations in T and S expectedly show a sizable impact of $\mathcal{K}_\sigma$, along with the predominant impact of $\mathcal{K}_{\mathsf{gm}}$ (Figs. 7–8). The existence of such contrasting dynamical regimes points to the importance of not overly simplifying the inversion problem and the underlying model.

4 Estimated turbulent transport parameters

The results from Sects. 2 and 3 suggest that the estimated $\mathcal{K}_{\mathsf{gm}}$, $\mathcal{K}_{\sigma}$ and $\mathcal{K}_{\mathsf{d}}$ may have oceanographic value beyond the ECCO v4 state estimate itself – a notion supported by Fig. 3 in particular. The main goal of this section is to further assert the relationship between the observed ocean stratification and estimated turbulent transport parameters, and to assess whether the estimated parameter maps are physically meaningful.

Each of the estimated parameters varies by orders of magnitudes on a regional basis, and thus shows a great degree of heterogeneity (Fig. 9) – a physically reasonable proposition (see, e.g. Eden, 2006; Eden et al., 2007; Fox-Kemper et al., 2013). Highs and lows often alternate at the same latitudes over extended regions. $\mathcal{K}_{\mathsf{gm}}$, $\mathcal{K}_{\sigma}$ and $\mathcal{K}_{\mathsf{d}}$ however also show extended regions of limited departure from K_{gm}, K_{σ} and K_{d} (regions in green). This behavior ought to be expected in regions where turbulent transports may be weak regardless of the corresponding coefficients.

Patterns of large parameter adjustments generally align with contours of observed stratification (Fig. 9). Stratification contrasts are indeed expected to delineate between regimes of turbulence, where one or another physical process may become predominant. Parameterized turbulent transports furthermore act along or across isopycnals, and stratification contrasts are indicators of the isopycnals geography.

Parameterized advection of tracers by meso-scale eddies (see Eq. 1) is controlled by $\mathcal{K}_{\mathsf{gm}}$. Reduction in $\mathcal{K}_{\mathsf{gm}}$ is most distinctly seen at the equatorward flank of the subtropical thermocline bowl in all oceanic basins (Fig. 9, top). Low $\mathcal{K}_{\mathsf{gm}}$ values appear consistent with the observed tropical thermocline characteristics (Figs. 1 and 6). The tropics are indeed known to show relatively low levels of meso-scale eddy activity and a predominance of baroclinic wave trains instead (e.g. Tulloch et al., 2009). The decrease from K_{gm} to $\mathcal{K}_{\mathsf{gm}}$ acts to increase the equatorward slant of isopycnals per Eq. (1).

Instances of $\mathcal{K}_{\mathsf{gm}} \geq K_{\mathsf{gm}}$ are common at higher latitudes where large isopycnal slopes are found. $\mathcal{K}_{\mathsf{gm}} > K_{\mathsf{gm}}$ is found at subpolar latitudes and not necessarily at the cores of the Antarctic Circumpolar Current (ACC) and subtropical jets. We refer the reader to Ferreira

et al. (2005) and Liu et al. (2012) for discussions of comparable results. Following the various ACC branches and meanders, instances of both $\mathcal{K}_{\mathsf{gm}} < K_{\mathsf{gm}}$ and $\mathcal{K}_{\mathsf{gm}} > K_{\mathsf{gm}}$ are found depending on longitude, as should be expected from Eden (2006) and subsequent studies. Furthermore, vertical contrasts in $\mathcal{K}_{\mathsf{gm}}$ are readily apparent in Fig. 9, such as the appearance of $\mathcal{K}_{\mathsf{gm}} > K_{\mathsf{gm}}$ patches in the ACC between 300 and 900 m depth. They become even more predominant at greater depths (see Sect. 5).

Isopycnal tracer diffusion due to lateral turbulence is controlled by $\mathcal{K}_\sigma$ (see Eq. 1). Similar adjustment patterns can be seen in $\mathcal{K}_\sigma$ (Fig. 9, middle) and $\mathcal{K}_{\mathsf{gm}}$ (Fig. 9, top). Notably $\mathcal{K}_\sigma$ shows minima in the tropics at 300m and below (in qualitative agreement with Cole et al., 2015) that correspond to $\mathcal{K}_{\mathsf{gm}}$ minima (see also Fig. 2). This is not entirely surprising since the two paramaterized processes, while generally distinct, are both associated with lateral turbulence, so that $\mathcal{K}_\sigma$ and $\mathcal{K}_{\mathsf{gm}}$ may covary (see, e.g. Abernathey et al., 2013). It should be noted however that the estimation settings did not impose covariance between the two parameters, but it is allowed to emerge from data constraints if adequate. Differences between $\mathcal{K}_\sigma$ and $\mathcal{K}_{\mathsf{gm}}$ could conversely indicate regions where the ocean state is not equally sensitive to the diffusive and advective effects of lateral turbulence.

One notable feature in $\mathcal{K}_\sigma$ (Fig. 9, middle right) that is not in $\mathcal{K}_{\mathsf{gm}}$ (Fig. 9, top right) is its reduction from K_σ near 900 m on the southern side of the ACC and near Antarctica (see also Fig. 2). It is physically reasonable that isopycnal diffusion is a particularly sensitive process in regions showing large tracer gradients along isopycnals (see Gnanadesikan et al., 2014). Also notable are two contrasting situations in the North Atlantic. The subpolar gyre shows increased $\mathcal{K}_{\mathsf{gm}}$ and $\mathcal{K}_\sigma$. The eastern subtropics at 900 m (near the Mediteranean outflow depth) show reduced $\mathcal{K}_{\mathsf{gm}}$ but increased $\mathcal{K}_\sigma$. As emphasized by Abernathey et al. (2013), $\mathcal{K}_{\mathsf{gm}}$ and $\mathcal{K}_\sigma$ are not expected to be equal except under specific limits. Gnanadesikan et al. (2014) further illustrate that tying $\mathcal{K}_\sigma$ strictly to $\mathcal{K}_{\mathsf{gm}}$ (as is often done in ocean modeling) can be problematic. The contrasted cases seen in Figs. 2 and 9 provide observational evidence that $\mathcal{K}_\sigma$ and $\mathcal{K}_{\mathsf{gm}}$ are not systematically tied to each other.

Background diapycnal diffusivity $\mathcal{K}_{\mathsf{d}}$ is increased from K_{d} at 300 m near 30° latitude (Fig. 9, bottom left). This geography qualitatively agrees with the fine-structure observed

by Argo (Fig. 1 in Whalen et al., 2012) and theoretical predictions of intensified parametric subharmonic instability (e.g. MacKinnon and Winters, 2005). However interleaving of weak and strong mixing layers is a common feature of the $\mathcal{K}_\mathrm{d}$ inverse estimate. Hence $\mathcal{K}_\mathrm{d}$ at 900 m (Fig. 9, bottom right) is rather reduced at 30° latitudes.

A pronounced interleaving is also seen in $\mathcal{K}_\mathrm{d}$ near the Equator (Fig. 10). Increased $\mathcal{K}_\mathrm{d}$ in the upper 100 m is consistent with the analysis of (amongst others) Moum et al. (2009) and found in all basins. A secondary $\mathcal{K}_\mathrm{d}$ maximum can be seen in the Pacific and Atlantic immediately underneath the Equatorial Under Curent. Shear instability is a good candidate mechanism also in this case. The deepest Pacific maximum (near 1000 m in Fig. 10) is a tropical rather than equatorial feature (Fig. 9, bottom right). Its dynamical origin is likely very different from the two upper maxima, and associated with the internal thermocline (see Sect. 3; Fig. 7).

In summary this section shows that the regional contrasts in $\mathcal{K}_\mathrm{gm}$, $\mathcal{K}_\sigma$ and $\mathcal{K}_\mathrm{d}$ are tied to regional stratification contrasts, and that these estimates generally are physically plausible. It is not implied however that turbulent transport rates are uniquely dependent on stratification alone and everywhere. The interplay of instability processes that in turn govern turbulent transports and stratification on a regional basis certainly remains a subject of active research of great importance beyond this paper. The presented analysis simply supports the notion that turbulent transport rates are effectively constrained (i.e. observable) by means of Argo's extensive collection of stratification profiles.

5 Assessment of uncertainties

A comparison of ECCO v4 parameter estimates (Figs. 9 and 11) with earlier inversion results that did not cover the Argo era (Ferreira et al., 2005; Stammer, 2005; Liu et al., 2012) should be indicative of overall observational uncertainty levels. None of the listed estimates is provided with a formal error estimate, which more generally remains a major caveat of ocean modeling and data synthesis. In such context inter-comparison of solutions is a com-

monly accepted, practical method to assess uncertainties even though its results are often difficult to interpret precisely (see Danabasoglu et al., 2014; Balmaseda et al., 2014).

In particular, attributing point by point differences amongst inverse estimates to specific causes would be a perilous exercise, due to various differences in model and estimation settings, and therefore no such attempt is made. It is worth highlighting, however, that ECCO v4 benefits from many innovations (e.g., updated numerics, the addition of a sea ice model and of the Arctic, and increased vertical resolution) as compared with previous generation model setups used by Ferreira et al. (2005), Stammer (2005), and Liu et al. (2012). A more exhaustive list of innovations is provided by Forget et al. (2015).

The most meaningful comparison maybe between the ECCO v4 and Liu et al. (2012) results since their respective experimental settings are most comparable. Importantly, estimated parameter adjustments are larger in ECCO v4 than in Liu et al. (2012) (compare Fig. 11 with Figs. 7c, 12b and 13b in Liu et al. 2012). It should be noted that the impact of the K_{gm}, K_σ and K_{d} adjustments in ECCO v4 was shown to generally exceed the impact of model errors unrelated to turbulent transport parameterizations (Forget et al., 2015). Therefore the increased parameter adjustment amplitude (in ECCO v4 as compared with Liu et al. 2012) is thought to primarily reflect the extensive data constraints added over 2002-2011 (see Fig. 5) rather than differences in model settings.

Regardless of the noted caveats, it is encouraging that ECCO v4 parameter estimates (Figs. 9 and 11) bear some resemblance to the Ferreira et al. (2005), Stammer (2005) and Liu et al. (2012) results, which may indicate robust oceanic features. All estimates are rich in regional adjustment patterns aligned with contours of the large-scale hydrography. The three $\mathcal{K}_{\mathsf{d}}$ estimates (Stammer, 2005; Liu et al., 2012 and ECCO v4) show elevated mixing near 30° latitude at 300 m, and interleaving of high and low mixing in the tropics. The $\mathcal{K}_{\mathsf{d}}$ map of Liu et al. (2012) at 300 m (their Fig. 7a) more generally is in a good qualitative agreement with Fig. 9 (bottom left). As a final example the three $\mathcal{K}_{\mathsf{gm}}$ estimates (Ferreira et al., 2005; Liu et al., 2012 and ECCO v4) show maxima associated with the ACC, minima in the tropics, and maxima in the North Atlantic subpolar gyre.

There are, however, also many differences amongst inverse parameter estimates. Firstly, ECCO v4 shows intensified diapycnal mixing in the tropical thermocline below 500m (Fig. 11; bottom panel) as compared with Stammer (2005) and Liu et al. (2012). Secondly, the three $\mathcal{K}_{\text{gm}}$ estimates largely differ in their magnitude and vertical structure in the ACC and at 40° N. Ferreira et al. (2005) show increased $\mathcal{K}_{\text{gm}}$ in the upper 1000 m in the ACC, with a near surface maximum, whereas Liu et al. (2012) and ECCO v4 (Fig. 11; top panel) show increased $\mathcal{K}_{\text{gm}}$ between 1000 and 3000 m. In the Gulf Stream, Ferreira et al. (2005) show a $\mathcal{K}_{\text{gm}}$ maximum in the upper 1000 m, whereas Liu et al. (2012) and ECCO v4 show $\mathcal{K}_{\text{gm}}$ minima at these depths. Also, neither Ferreira et al. (2005) nor Liu et al. (2012) show the increased $\mathcal{K}_{\text{gm}}$ seen near the coast of Antarctica in ECCO v4. Finally, K_σ in ECCO v4 (Fig. 11; middle panel) hints at a steering level effect (Green, 1970; Abernathey et al., 2010; Ferrari and Nikurashin, 2010) below 500m in the ACC that is not seen in Liu et al. (2012). Such differences are indicative of large overall uncertainty in inverse parameter estimates.

Furthermore, regions where parameters remain virtually unadjusted (Figs. 2 and 9; regions in green) likely denote large uncertainties reflecting that available data constraints are insufficiently sensitive to prompt sizable parameter adjustments (as noted by Liu et al., 2012). The relatively weak values of $\mathcal{K}_{\text{d}} - K_{\text{d}}$ in the ACC (as compared with, e.g., Whalen et al. 2012, but not with Liu et al. 2012) may be one example. Similarly the fact that $\mathcal{K}_{\text{d}} - K_{\text{d}}$ is generally muted in the abyss (albeit with notable exceptions in the Southern Ocean) is not surprising, and does not imply that K_{d} is a precise first guess. Indeed the equilibration of the abyssal stratification (or the lack thereof) and the recycling of abyssal water masses are dominated by very long time scales, and abyssal observations are very sparse as compared with upper ocean data constraints.

It is in fact encouraging that $\mathcal{K}_{\text{d}}$ shows even marginal increases near the sea floor (Figs. 12, right and 2, bottom right) as it is often expected to result from the interaction of barotropic tides (amongst others) and bottom topography (Polzin et al., 1997; Ledwell et al., 2000; Naveira Garabato et al., 2004; Sloyan, 2005). It is intriguing that low K_{d} values are also found near the bottom – mostly in the Southern Ocean along deep canyon margins (Figs. 12, right and Fig. 2, bottom left). However reductions in diapycnal diffusivity

(from K_{d} to $\mathcal{K}_{\mathrm{d}}$) may compensate for an unknown amount of numerical diffusion implied by the advection schemes, and bottom boundary layers are notoriously difficult to simulate adequately in ocean models. For these reasons, and since they are not seen in Stammer (2005) or Liu et al. (2012), the $\mathcal{K}_{\mathrm{d}}$ contrasts in Fig. 12 should be interpreted most cautiously.

The deep Southern Ocean can adjust relatively fast due to the proximity of bottom water formation sites and the presence of a deep wind- and eddy-driven thermocline (see Karsten and Marshall, 2002) that result in a strong coupling of superficial and deep layers in the ACC region (see Fig. 7). Hence the large values of $\mathcal{K}_{\mathrm{gm}}$ at 3000 m estimated over 20 years in the Southern Ocean may be physically meaningful (Fig. 12, left). Maxima in $\mathcal{K}_{\mathrm{gm}}$ are located along the ACC path just downstream of Kerguelen and at Drake passage, as well as in the Brazil–Malvinas confluence region, in the Ross Sea and in the Weddell Sea. These regions are indeed characterized by relatively large isopycnal slopes, and eddying numerical models show sizable meso-scale eddy activity even at 3000 m along the ACC (Ponte, 2012). It will be interesting to see whether the $\mathcal{K}_{\mathrm{gm}}$ maxima seen in Fig. 12 are confirmed (or otherwise) in inversion experiments conducted once deep Argo profiles are available.

6 Summary and perspectives

This study asserts that extended observation of the broad-scale hydrography by Argo should translate into improved inverse estimates of regional turbulent transport rates in the upper 2000 m over the global ocean. Time-invariant three-dimensional maps of turbulent transport parameters ($\mathcal{K}_{\mathrm{gm}}$, $\mathcal{K}_{\sigma}$ and $\mathcal{K}_{\mathrm{d}}$) are estimated as part of ECCO v4 (Forget et al., 2015) and under the observational constraint of Argo T-S profiles collected through 2011. The presented exploration of the method of turbulent transport parameter inversion, while still incomplete, fills a major gap in the oceanographic literature.

The observability of turbulent transport rates is asserted by focusing on ocean stratification ($\frac{\partial \rho}{\partial z}$ and mixed layer depths). Argo indeed readily observes these key oceanographic variables with un-precedented data coverage. The estimated turbulent transport parameters

are consistent with the observed stratification by construction, since it is well reproduced by the ECCO v4 ocean state estimate. It is shown that ocean stratification over the upper 2000 m is highly sensitive to the estimated parameter adjustments, and that the geography of estimated parameter adjustments is aligned with contours of observed ocean stratification. Thus, the constraint of fitting Argo profiles is identified as an effective observational basis for the inversion of turbulent transport parameters.

As part of the inversion method evaluation it is shown that the estimated parameters reduce spurious model drifts (i.e. accumulating model biases) of the physical ocean state in multi-century simulations. They also lead to remarkable improvements in simulating biogeochemistry variables that were not involved in the parameters optimization. The estimated parameter adjustments themselves and the resulting adjustments in ocean stratification are physically plausible despite the minimal constraints that were built in the optimization. These results demonstrate that the estimated parameters have intrinsic value beyond the optimized solution of the 20 year evolving ocean physical state.

The asserted "observability" of turbulent transport rates by Argo does not, however, require or imply that the present parameter estimates are very precise or accurate. Given the noted contrasts amongst published inversion results, and given that vast regions show negligible parameter adjustments, it is unlikely that available T-S profiles suffice to determine regional turbulent transport rates uniquely and everywhere. The overall weakness of estimated parameter adjustments in the abyss is also revealing of current limitations – extensive Argo data collection has only reached 2000 m and 20 years is too short to fully resolve (im)balances of the abyss. Additional observational constraints (e.g. passive and biogeochemical tracer observations), statistical constraints (e.g. observed fine-scale and meso-scale statistics) and dynamical constraints (e.g. longer time scales, energetics) ought to complement the constraint of T-S profiles in future inversion experiments.

The lack of a practical technology to associate estimated turbulent transport parameters with formal error estimates is arguably the main caveat here as well as in Stammer (2005), Ferreira et al. (2005), and Liu et al. (2012). It is the reason why observability of turbulent transport rates by means of Argo and other global data sets largely remains to be quantified.

The presented inter-comparison of inversion results, however, provides clues into overall levels of uncertainty. The closest agreement appears to be between $\mathcal{K}_{\mathrm{d}}$ estimates at 300 m. A much more contrasted picture emerges for e.g. $\mathcal{K}_{\mathrm{gm}}$ in the main mid-latitude jets (ACC, Gulf Stream, Kuroshio). The three inverse estimates of $\mathcal{K}_{\mathrm{gm}}$ (Ferreira et al., 2005; Liu et al., 2012; Forget et al., 2015) show both minima and maxima along or near the jets, but with differences in their geographic and vertical distributions.

Aside from the need for formal error estimates, and additional constraints, much remains to be done to refine inverse estimates of turbulent transport rates, and our understanding of their observability. One practical approach would consist in conducting twin estimation experiments (see, e.g. Forget et al., 2008a) focusing on turbulent transport parameter inversions. Another one would consist in conducting dedicated estimation experiments where real data sets are withheld or added one at a time to further compare the constraints that they respectively provide (see, e.g. Forget et al., 2008b). And the presented results should eventually be re-evaluated on the basis of additional estimation experiments that would differ from Forget et al. (2015) in regard of parameter ranges, first guess values, and error covariance specifications (that all are uncertain estimation settings).

Ongoing research aiming to diagnose and alleviate numerical diffusion (e.g. Hill et al., 2012) and structural model uncertainty (Forget et al., 2015) is of direct relevance to turbulent transport parameter inversions. Numerical diffusivity of advection schemes or e.g. momentum equation biases could very well contaminate turbulent transport parameter estimates. Forget et al. (2015) show that turbulent transport parameter adjustments exceed what may be expected to compensate for model errors due to advection and momentum scheme choices. However, turbulent transport parameter inversions will need to be conducted with a variety of numerical models before one can reach more definitive conclusions in this regard. To start it will be interesting to see how much of the beneficial impacts of the presented $\mathcal{K}_{\mathrm{gm}}$, $\mathcal{K}_{\sigma}$ and $\mathcal{K}_{\mathrm{d}}$ carries over to different ocean and climate models.

Acknowledgements. G. Forget expresses his gratitude to Jean Michel Campin, Patrick Heimbach and Christopher N. Hill for the technical help they provided during the development of ECCO v4. To Carl Wunsch and Ryan Abernathey for useful comments on the presented analysis. To Jane

Chapin for useful editorial comments. Efforts of G. Forget and X. Liang were supported in part by National Science Foundation through Grant OCE-0961713 and National Oceanic and Atmospheric Administration through Grant NA10OAR4310135.

References

Abernathey, R., Ferreira, D., and Klocker, A.: Diagnostics of isopycnal mixing in a circumpolar channel, Ocean Model., 72, 1–16, 2013.

Abernathey, R., Marshall, J., Shuckburgh, E., Mazloff, M.: Enhancement of mesoscale eddy stirring at steering levels in the Southern Ocean. J. Phys. Oceanogr., 170?185, 2010.

Abernathey, R. and Marshall, J.: Global surface eddy diffusivities derived from satellite altimetry, J. Geophys. Res.-Oceans, 118, 901–916, 2013.

Abernathey, R., Ferreira, D., and Klocker, A.: Diagnostics of isopycnal mixing in a circumpolar channel, Ocean Model., 72, 1–16, 2013.

Balmaseda, M., Hernandez, F., Storto, A., Palmer, M., Alves, O., Shi, L., Smith, G., Toyoda, T., Valdivieso, M., Barnier, B., Behringer, D., Boyer, T., Chang, Y.-S., Chepurin, G., Ferry, N., Forget, G., Fujii, Y., Good, S., Guinehut, S., Haines, K., Ishikawa, Y., Keeley, S., Kohl, A., Lee, T., Martin, M., Masina, S., Masuda, S., Meyssignac, B., Mogensen, K., Parent, L., Peterson, K., Tang, Y., Yin, Y., Vernieres, G., Wang, X., Waters, J., Wedd, R., Wang, O., Xue, Y., Chevallier, M., Lemieux, J.-F., Dupont, F., Kuragano, T., Kamachi, M., Awaji, T., Caltabiano, A., Wilmer-Becker, K., and Gaillard, F.: The Ocean Reanalyses Intercomparison Project (ORA-IP), Proceedings of the Institute of Marine Engineering, Science, and Technology, J. Operational Oceanogr., 8, s80–s97, doi:10.1080/1755876X.2015.1022329, 2015.

Cole, S. T., Wortham, C., Kunze, E., and Owens, W. B.: Eddy stirring and horizontal diffusivity from Argo float observations: Geographic and depth variability. Geophys. Res. Lett., 42, 3989?3997, doi:10.1002/2015GL063827, 2015

Danabasoglu, G. and Marshall, J.: Effects of vertical variations of thickness diffusivity in an ocean general circulation model, Ocean Model., 18, 122–141, 2007.

Danabasoglu, G., Yeager, S. G., Bailey, D., Behrens, E., Bentsen, M., Bi, D., Biastoch, A., Böning, C., Bozec, A., Canuto, V. M., Cassou, C., Chassignet, E., Coward, A. C., Danilov, S., Diansky, N., Drange, H., Farneti, R., Fernandez, E., Fogli, P. G., Forget, G., Fujii, Y., Griffies, S. M., Gusev, A., Heimbach, P., Howard, A., Jung, T., Kelley, M., Large, W. G., Leboissetier, A., Lu, J., Madec, G.,

Marsland, S. J., Masina, S., Navarra, A., Nurser, A. G., Pirani, A., Salas y Mélia, D., Samuels, B. L., Scheinert, M., Sidorenko, D., Treguier, A.-M., Tsujino, H., Uotila, P., Valcke, S., Voldoire, A., and Wang, Q.: North Atlantic simulations in Coordinated Ocean-ice Reference Experiments phase {II} (CORE-II). Part I: Mean states, Ocean Model., 73, 76–107, doi:10.1016/j.ocemod.2013.10.005, 2014.

Duffy, P., Eby, M., and Weaver, A.: Effects of sinking of salt rejected during formation of sea ice on results of an ocean–atmosphere–sea ice climate model, Geophys. Res. Lett., 26, 1739–1742, 1999.

Dutkiewicz, S., Sokolov, A. P., Scott, J., and Stone, P. H.: A three-dimensional ocean-seaice-carbon cycle model and its coupling to a two-dimensional atmospheric model: uses in climate change studies, MIT Joint Program on the Science and Policy of Global Change, 2005.

Eden, C.: Thickness diffusivity in the Southern Ocean, Geophys. Res. Lett., 33, L11606 doi:10.1029/2006GL026157, 2006.

Eden, C., Greatbatch, R. J., and Willebrand, J.: A diagnosis of thickness fluxes in an eddy-resolving model, J. Phys. Oceanogr., 37, 727–742, 2007.

Eden, C., Jochum, M., and Danabasoglu, G.: Effects of different closures for thickness diffusivity, Ocean Model., 26, 47–59, 2009.

England, M. H.: Representing the global-scale water masses in ocean general circulation models, J. Phys. Oceanogr., 23, 1523–1552, 1993.

Ferreira, D., Marshall, J., and Heimbach, P.: Estimating eddy stresses by fitting dynamics to observations using a residual-mean ocean circulation model and its adjoint., J. Phys. Oceanogr., 35, 1891–1910, 2005.

Forget, G.: Mapping ocean observations in a dynamical framework: a 2004–06 ocean atlas, J. Phys. Oceanogr., 40, 1201–1221, 2010.

Forget, G. and Ponte, R.: The partition of regional sea level variability, Prog. Oceanogr., 137, 173–195, doi:10.1016/j.pocean.2015.06.002, 2015.

Forget, G. and Wunsch, C.: Estimated global hydrographic variability, J. Phys. Oceanogr., 37, 1997–2008, 2007.

Forget, G., Ferron, B., and Mercier, H.: Combining Argo profiles with a general circulation model in the North Atlantic. Part 1: Estimation of hydrographic and circulation anomalies from synthetic profiles, over a year, Ocean Model., 20, 1–16, 2008a.

Forget, G., Mercier, H., and Ferron, B.: Combining Argo profiles with a general circulation model in the North Atlantic. Part 2: Realistic transports and improved hydrography, between spring 2002 and spring 2003, Ocean Model., 20, 17–34, 2008b.

Forget, G., Campin, J.-M., Heimbach, P., Hill, C. N., Ponte, R. M, and Wunsch, C.: ECCO version 4: an integrated framework for non-linear inverse modeling and global ocean state estimation, Geosci. Model Dev. Discuss., 8, 3653–3743, doi:10.5194/gmdd-8-3653-2015, 2015.

Fox-Kemper, B., Lumpkin, R., and Bryan, F.: Lateral transport in the ocean interior, in: Ocean Circulation and Climate: a 21st Century Perspective, International Geophysics, Elsevier Science, 185–209, 2013.

Ganachaud, A.: Large-scale mass transports, water mass formation, and diffusivities estimated from World Ocean Circulation Experiment (WOCE) hydrographic data, J. Geophys. Res.-Oceans, 108, 3213, doi:10.1029/2002JC001565, 2003.

Garcia, H., Locarnini, R., Boyer, T., Antonov, J., Zweng, M., Baranova, O., and Johnson, D.: World Ocean Atlas 2009, vol. 4, Nutrients (Phosphate, Nitrate, Silicate), edited by: Levitus, S., NOAA Atlas NESDIS, 71, 2010.

Gaspar, P., Grégoris, Y., and Lefevre, J.-M.: A simple eddy kinetic energy model for simulations of the oceanic vertical mixing: tests at Station Papa and long-term upper ocean study site, J. Geophys. Res., 95, 16179–16193, 1990.

Gent, P. and Mcwilliams, J.: Isopycnal mixing in ocean circulation models, J. Phys. Oceanogr., 20, 150–155, 1990.

Gnanadesikan, A., Abernathey, R., and Pradal, M.-A.: Exploring the isopycnal mixing and helium-heat paradoxes in a suite of Earth System Models, Ocean Sci. Discuss., 11, 2533–2567, doi:10.5194/osd-11-2533-2014, 2014.

Green, J. S.: Transfer properties of the large-scale eddies and the general circulation of the atmosphere. Quart. J. Roy. Meteor. Soc., 96, 157–185, 1970

Griffies, S. M., Adcroft, A. J., Banks, H., Boning, C. W., Chassignet, E. P., Danabasoglu, G., Danilov, S., Deelersnijder, E., Drange, H., England, M., Fox-Kemper, B., Gerdes, R., Gnanadesikan, A., Greatbatch, R. J., Hallberge, R. W., Hanert, E., Harrison, M. J., Legg, S., Little, C. M., Madec, G., Marsland, S. J., Nikurashin, M., Pirani, A., Simmons, H. L., Schroter, J., Samuels, B. L., Treguier, A.-M., Toggweiler, J. R., Tsujino, H., Vallis, G. K., and White, L.: Problems and prospects in large-scale ocean circulation models, in: OceanObs' 09 Conference: Sustained Ocean Observations and Information for Society, Venice, Italy, 21–25 September 2009, 2, 1–24, 2010.

Hill, C., Ferreira, D., Campin, J.-M., Marshall, J., Abernathey, R., and Barrier, N.: Controlling spurious diapycnal mixing in eddy-resolving height-coordinate ocean models – insights from virtual deliberate tracer release experiments, Ocean Model., 45, 14–26, 2012.

Iselin, C.: The influence of vertical and lateral turbulence on the characteristics of the waters at mid-depths, EOS T. Am. Geophys. Un., 20, 414–417, 1939.

Iselin, C. O.: A study of the circulation of the western North Atlantic, Massachusetts Institute of Technology and Woods Hole Oceanographic Institution, Cambridge, Massachusetts, 1936.

Jochum, M., Briegleb, B. P., Danabasoglu, G., Large, W. G., Norton, N. J., Jayne, S. R., Alford, M. H., and Bryan, F. O.: The impact of oceanic near-inertial waves on climate, J. Climate, 26, 2833–2844, 2013.

Karsten, R. H. and Marshall, J.: Constructing the residual circulation of the ACC from observations, J. Phys. Oceanogr., 32, 3315–3327, 2002.

Key, R. M., Kozyr, A., Sabine, C. L., Lee, K., Wanninkhof, R., Bullister, J. L., Feely, R. A., Millero, F. J., Mordy, C., and Peng, T.-H.: A global ocean carbon climatology: results from Global Data Analysis Project (GLODAP), Global Biogeochem. Cy., 18, GB4031, doi:10.1029/2004GB002247, 2004.

Krauß, W., and Böning, C. W.: Lagrangian properties of eddy fields in the northern North Atlantic as deduced from satellite-tracked buoys, J. Mar. Res., 45, 259–291, 1987.

Ledwell, J., Montgomery, E., Polzin, K., Laurent, L. S., Schmitt, R., and Toole, J.: Evidence for enhanced mixing over rough topography in the abyssal ocean, Nature, 403, 179–182, 2000.

Ledwell, J. R., Watson, A. J., and Law, C. S.: Evidence for slow mixing across the pycnocline from an open-ocean tracer-release experiment, Nature, 364, 701–703, 1993.

Ledwell, J. R., Watson, A. J., and Law, C. S.: Mixing of a tracer in the pycnocline, J. Geophys. Res.-Oceans, 103, 21499–21529, 1998.

Liu, C., Köhl, A., and Stammer, D.: Adjoint-based estimation of eddy-induced tracer mixing parameters in the global ocean, J. Phys. Oceanogr., 42, 1186–1206, 2012.

Lumpkin, R. and Speer, K.: Global ocean meridional overturning, J. Phys. Oceanogr., 37, 2550–2562, 2007.

Luyten, J., Pedlosky, J., and Stommel, H.: The ventilated thermocline, J. Phys. Oceanogr., 13, 292–309, 1983.

MacKinnon, J. and Winters, K.: Subtropical catastrophe: significant loss of low-mode tidal energy at 28.9, Geophys. Res. Lett., 32, L15605, doi:10.1029/2005GL023376, 2005.

MacKinnon, J., St Laurent, L., and Naveira Garabato, C.: Diapycnal mixing processes in the ocean interior, in: Ocean Circulation and Climate: a 21st Century Perspective, International Geophysics, Elsevier Science, 159–184, 2013.

Marshall, J., Shuckburgh, E., Jones, H., and Hill, C.: Estimates and implications of surface eddy diffusivity in the Southern Ocean derived from tracer transport, J. Phys. Oceanogr., 36, 1806–1821, 2006.

McDougall, T. J.: The relative roles of diapycnal and isopycnal mixing on subsurface water mass conversion, J. Phys. Oceanogr., 14, 1577–1589, 1984.

Melet, A., Hallberg, R., Legg, S., and Nikurashin, M.: Sensitivity of the ocean state to lee wave–driven mixing, J. Phys. Oceanogr., 44, 900–921, 2014.

Moum, J., Lien, R.-C., Perlin, A., Nash, J., Gregg, M., and Wiles, P.: Sea surface cooling at the equator by subsurface mixing in tropical instability waves, Nat. Geosci., 2, 761–765, 2009.

Munk, W. and Wunsch, C.: Abyssal recipes II: energetics of tidal and wind mixing, Deep-Sea Res. Pt. I, 45, 1977–2010, 1998.

Munk, W. H.: Abyssal recipes, in: Deep Sea Research and Oceanographic Abstracts, vol. 13, Elsevier, 707–730, 1966.

Naveira Garabato, A. C., Polzin, K. L., King, B. A., Heywood, K. J., and Visbeck, M.: Widespread intense turbulent mixing in the Southern Ocean, Science, 303, 210–213, 2004.

Ferrari, R. and Nikurashin, M.: Suppression of eddy diffusivity across jets in the Southern Ocean. J. Phys. Oceanogr., 40, 1501–1519, 2010.

Olbers, D., Wenzel, M., and Willebrand, J.: The inference of North Atlantic circulation patterns from climatological hydrographic data, Rev. Geophys., 23, 313–356, 1985.

Polzin, K., Toole, J., Ledwell, J., and Schmitt, R.: Spatial variability of turbulent mixing in the abyssal ocean, Science, 276, 93–96, 1997.

Ponte, R. M.: An assessment of deep steric height variability over the global ocean, Geophys. Res. Lett., 39, L04601, doi:10.1029/2011GL050681, 2012.

Redi, M. H.: Oceanic isopycnal mixing by coordinate rotation, J. Phys. Oceanogr., 12, 1154–1158, 1982.

Roemmich, D., Boebel, O., Desaubies, Y., Freeland, H., King, B., LeTraon, P.-Y., Molinari, R., Owens, B., Riser, S., Send, U., Kensuke, T., and Wijffels, S.: ARGO: the Global Array of Profiling Floats, CLIVAR Exchanges, 13, 4–5, 1999.

Roemmich, D., Johnson, G. C., Riser, S., Davis, R., Gilson, J., Owens, W. B., Garzoli, S. L., Schmid, C., and Ignaszewski, M.: The Argo Program: observing the global ocean with profiling floats, 2009.
Samelson, R. and Vallis, G. K.: Large-scale circulation with small diapycnal diffusion: the two-thermocline limit, J. Mar. Res., 55, 223–275, 1997.
Schott, F. and Zantopp, R.: On the effect of vertical mixing on the determination of absolute currents by the beta spiral method, Deep-Sea Res., 27, 173–180, 1980.
Siedler, G., Griffies, S., Gould, J., and Church, J.: Ocean Circulation and Climate: a 21st Century Perspective, International Geophysics, Elsevier Science, 2013.
Sloyan, B. M.: Spatial variability of mixing in the Southern Ocean, Geophys. Res. Lett., 32, L18603, doi:10.1029/2005GL023568, 2005.
Speer, K. and Forget, G.: Global distribution and formation of mode waters, in: Ocean Circulation and Climate: a 21st Century Perspective, International Geophysics, Elsevier Science, 211–226, doi:10.1016/B978-0-12-391851-2.00009-X, 2013.
Stammer, D.: Adjusting internal model errors through ocean state estimation, J. Phys. Oceanogr., 35, 1143–1153, 2005.
Toggweiler, J. and Samuels, B.: On the ocean's large-scale circulation near the limit of no vertical mixing, J. Phys. Oceanogr., 28, 1832–1852, 1998.
Tomczak, M. and Large, D. G.: Optimum multiparameter analysis of mixing in the thermocline of the eastern Indian Ocean, J. Geophys. Res.-Oceans, 94, 16141–16149, 1989.
Tulloch, R., Marshall, J., and Smith, K. S.: Interpretation of the propagation of surface altimetric observations in terms of planetary waves and geostrophic turbulence, J. Geophys. Res.-Oceans, 114, C02005, doi:10.1029/2008JC005055, 2009.
Tziperman, E.: On the role of interior mixing and air–sea fluxes in determining the stratification and circulation of the oceans, J. Phys. Oceanogr., 16, 680–693, 1986.
Vallis, G. K.: Atmospheric and Oceanic Fluid Dynamics: Fundamentals and Large-Scale Circulation, Cambridge University Press, Cambridge, UK, 2006.
Walin, G.: On the relation between sea-surface heat flow and thermal circulation in the ocean, Tellus, 34, 187–195, 1982.
Waterhouse, A. F., MacKinnon, J. A., Nash, J. D., Alford, M. H., Kunze, E., Simmons, H. L., Polzin, K. L., St. Laurent, L. C., Sun, O. M., Pinkel, R., Talley, L. D., Whalen, C. B., Huussen, T. N., Carter, G. S., Fer, I., Waterman, S., Naveira Garabato, A. C., Sanford, T. B., and Lee, C. M.:

Global patterns of diapycnal mixing from measurements of the turbulent dissipation rate, J. Phys. Oceanogr., 44, 1854–1872, 2014.

Webb, D. and Suginohara, N.: Oceanography: vertical mixing in the ocean, Nature, 409, 37–37, 2001.

Whalen, C., Talley, L., and MacKinnon, J.: Spatial and temporal variability of global ocean mixing inferred from Argo profiles, Geophys. Res. Lett., 39, L18612, doi:10.1029/2012GL053196, 2012.

Wu, L., Jing, Z., Riser, S., and Visbeck, M.: Seasonal and spatial variations of Southern Ocean diapycnal mixing from Argo profiling floats, Nat. Geosci., 4, 363–366, 2011.

Wunsch, C. and Heimbach, P.: Dynamically and kinematically consistent global ocean circulation and ice state estimates, in: Ocean Circulation and Climate: a 21st Century Perspective, International Geophysics, Elsevier Science, 553–579, 2013.

Wyrtki, K.: The oxygen minima in relation to ocean circulation, in: Deep Sea Research and Oceanographic Abstracts, vol. 9, Elsevier, 11–23, 1962.

Zika, J. D., Sloyan, B. M., and McDougall, T. J.: Diagnosing the Southern Ocean overturning from tracer fields, J. Phys. Oceanogr., 39, 2926–2940, 2009.

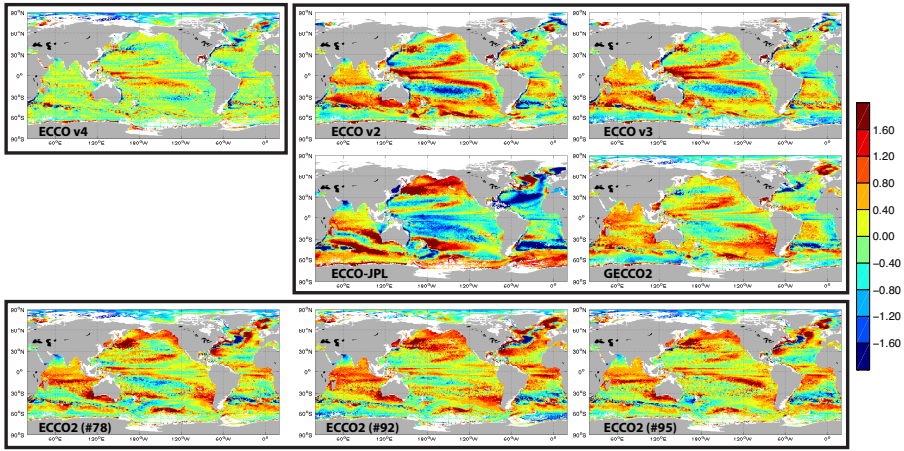

Figure 1. Model-data misfits for temperature at 300 m depth (color scale in °C). The ECCO v4 state estimate (Forget et al., 2015) used in this study is shown in the top left panel. The four panels in the top-right corner show earlier ECCO state estimates that use comparably coarse resolution grids (typically 1° as in ECCO v4). The ECCO v2, ECCO v3, and GECCO2 forcing fields were optimized using the adjoint method, whereas ECCO-JPL used a Kalman smoother instead. Unlike ECCO v4, these solutions use un-optimized turbulent transport parameters. The bottom three panels show ECCO2 eddying model solutions (with $\approx 1/6^\circ$ resolution) that use different sets of forcing fields. Further details on the solutions and these misfits can be found in Forget et al. (2015).

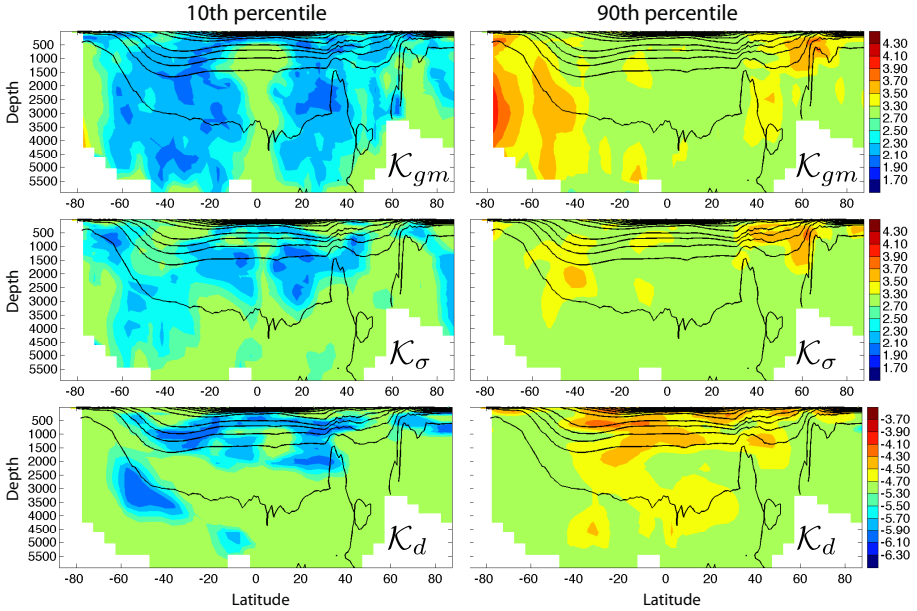

Figure 2. Estimated bolus velocity coefficient (top; $\mathcal{K}_{\mathrm{gm}}$), isopycnal diffusivity (middle; $\mathcal{K}_{\sigma}$) and diapycnal diffusivity (bottom; $\mathcal{K}_{\mathrm{d}}$) in $\mathrm{m}^2\,\mathrm{s}^{-1}$ ($\log_{10}$ color scale). Left: 10th percentile at each latitude and depth; right: 90th percentile. Overlaid black contours denote the time mean zonal mean potential density from the OCCA atlas (Forget, 2010).

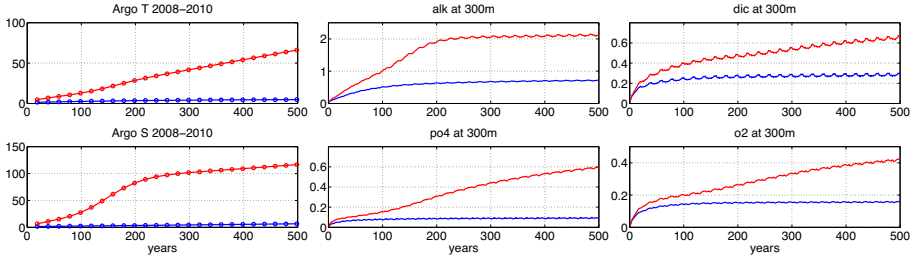

Figure 3. Long term model drifts away from the observed state gauged by repeated comparison with Argo profiles collected over 2008–2010 (top left: T; bottom left: S) and independent climatological data for biogeochemistry (middle and right panels) in simulations with (blue) the $\mathcal{K}_{\mathrm{gm}}$, $\mathcal{K}_\sigma$ and $\mathcal{K}_{\mathrm{d}}$ estimated parameter maps or (red) the K_{gm}, K_σ and K_{d} constant first guess parameters. Each plotted value is a cost function $\overline{d^2/\sigma^2}$ where d is a model–data difference, σ is an uncertainty estimate, and the overbar denotes averaging over all data points. Values of one would indicate model–data differences that are on average exactly at the estimated level of uncertainty. Argo cost function details are reported in Forget et al. (2015). The biogeochemistry model is from Dutkiewicz et al. (2005) with settings provided by H. Song (personal communication, 2015). The corresponding cost functions compare annual mean biogeochemistry model fields at 300 m with the climatologies that were used to initialize the model. The 300 m climatology standard deviation is further used as an ad-hoc uncertainty estimate to form a cost function. Top middle: alkalinity (Key et al., 2004); bottom middle: phosphate (Garcia et al., 2010); top right: dissolved inorganic carbon (Key et al., 2004); bottom right: dissolved oxygen (Garcia et al., 2010).

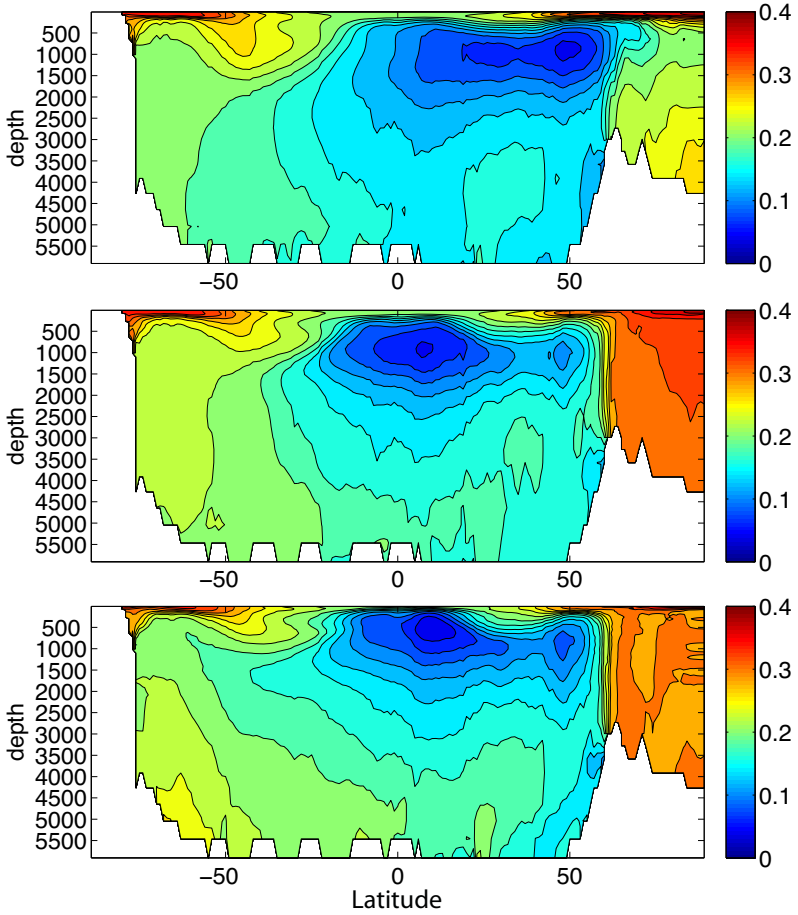

Figure 4. Zonal mean oxygen concentration (in $\mathrm{mol\,m^{-3}}$) from Garcia et al. (2010) (bottom panel) and from the two 500 years simulations (see Fig. 3 caption for details) using the $\mathcal{K}_{\mathrm{gm}}$, $\mathcal{K}_{\sigma}$, $\mathcal{K}_{\mathrm{d}}$ estimate (middle) or the K_{gm}, K_{σ}, K_{d} first guess (top).

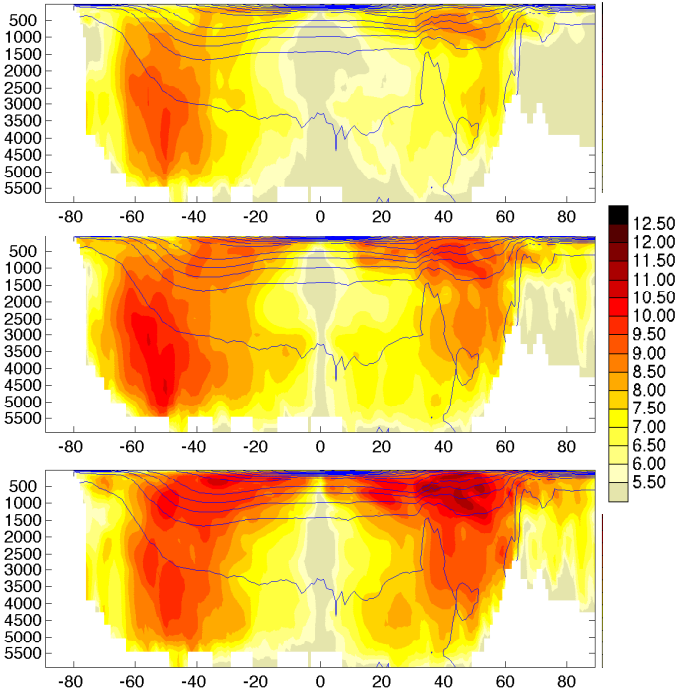

Figure 5. Sensitivity to $\mathcal{K}_{\text{gm}}$ associated with 1992-2001 altimetry (top), 1992-2011 altimetry (middle), and Argo T and S profiles (bottom). More than 98% of Argo profiles were collected after 2001. In each case, the squared model-data distance J is selected accordingly, and $\frac{\partial J}{\partial K_{\text{gm}}}$ is computed with the adjoint model. The adjoint model and J_{Argo} are documented in details in Forget et al. (2015). For altimetry, J uses the large-scale formulation of Forget and Ponte (2015). In all cases, turbulent optimization parameters are reset to their unadjusted values, so that the adjoint computation is representative of the starting point of the estimation process. The results are displayed non-dimensionally as $log_{10}(||u_{\text{gm}} \frac{\partial J}{\partial K_{\text{gm}}}||^2)$ where $||\,.\,||^2$ denotes the zonal mean squared norm, and $u_{\text{gm}} = 500$ m^2 s^{-1}.

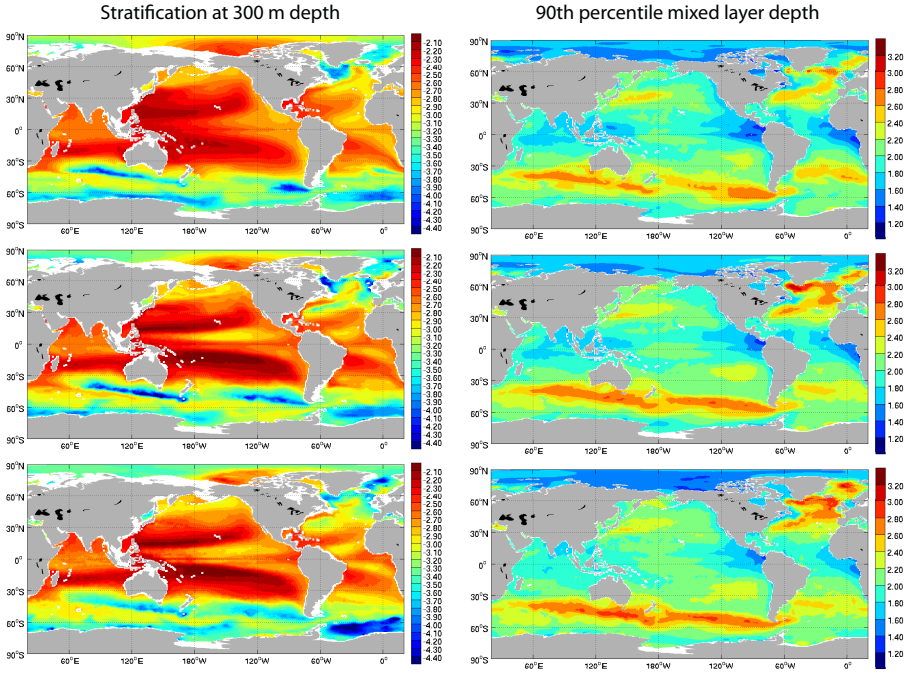

Figure 6. (Left) median stratification at 300 m depth (shown as $\log_{10}(\frac{\partial \rho}{\partial z})$ in kg m^{-4}) and (right) 90 percentile mixed layer depth (shown as $\log_{10}$(mld) in m) for (bottom) in situ profiles, (middle) the corresponding state estimate profiles, and (top) model profiles generated by resetting $\mathcal{K}_{\mathrm{gm}}$, $\mathcal{K}_{\sigma}$, $\mathcal{K}_{\mathrm{d}}$ to the K_{gm}, K_{σ}, K_{d} first guess while retaining all other settings of the state estimate. Percentiles are computed from the distribution of individual profile values within grid boxes and mapped.

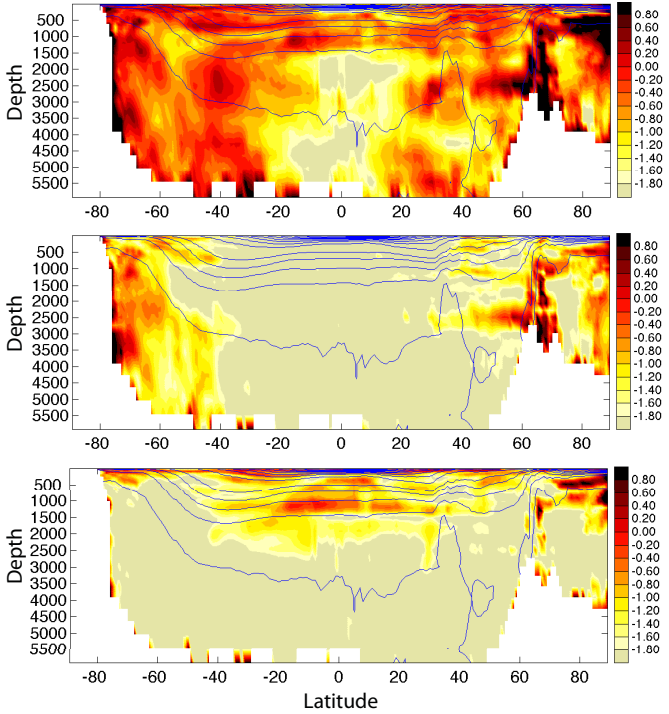

Figure 7. Sensitivity of ocean stratification to $\mathcal{K}_{\text{gm}}$ (top), $\mathcal{K}_\sigma$ (middle), and $\mathcal{K}_{\text{d}}$ (bottom). Mean squared deviations are computed between perturbation experiments and the state estimate for the 2008–2010 monthly climatology of $\frac{\partial \rho}{\partial z}$, and then normalized by the corresponding state estimate variance. The color shading shows the $\log_{10}$ of this ratio. Thus, orange denotes $> 10\,\%$ differences, while dark red denotes $> 100\,\%$ differences. The perturbation experiment where the $\mathcal{K}_{\text{gm}}$ (resp. $\mathcal{K}_\sigma$, $\mathcal{K}_{\text{d}}$) estimate is reset to the constant K_σ (resp. K_σ, K_{d}) first guess is shown at the top (resp. middle, bottom). Overlaid contours: zonal mean potential density from the OCCA atlas.

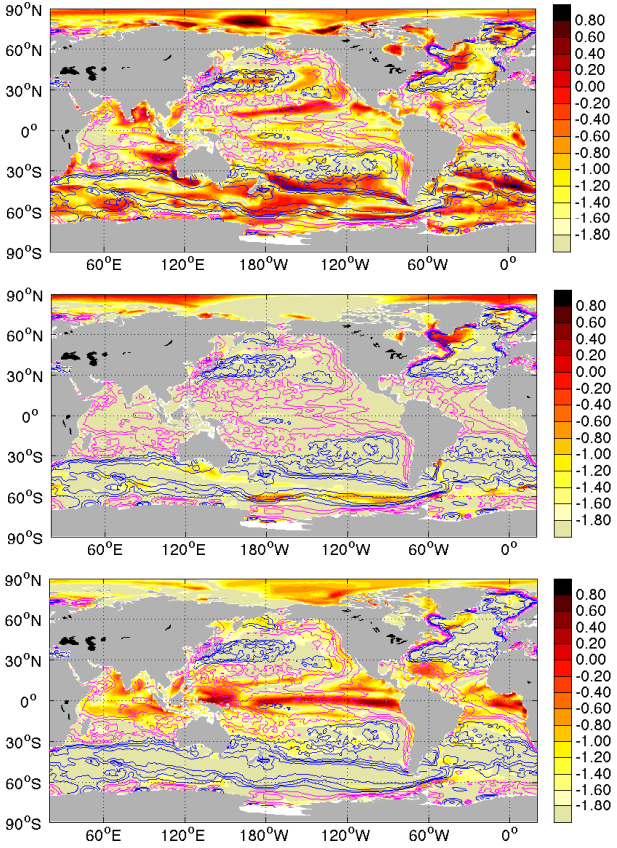

Figure 8. Mixed layer depth sensitivity (color shading) to $\mathcal{K}_{\text{gm}}$ (top), $\mathcal{K}_\sigma$ (middle), and $\mathcal{K}_{\text{d}}$ (bottom). Computational and plotting details are similar to Fig. 7. Overlaid blue contours (resp. magenta contours) denote the 60, 70, 80, 90th (resp. 10, 20, 30, 40th) percentiles of the observed mixed layer depth map (mld(x, y) from the bottom right panel of Fig. 6).

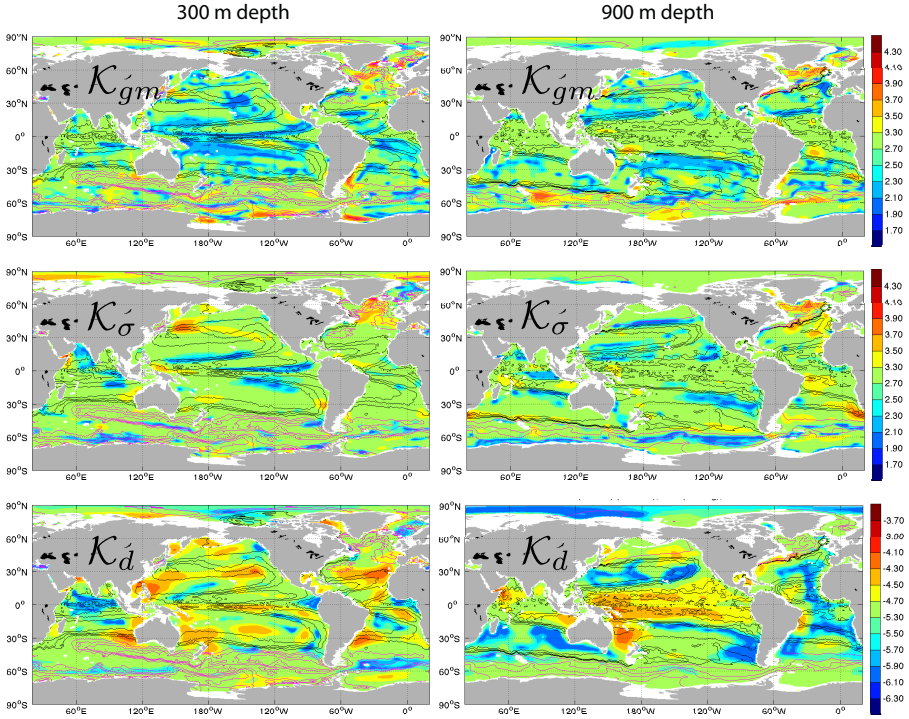

Figure 9. Estimated bolus velocity coefficient (top), isopycnal diffusivity (middle) and diapycnal diffusivity (bottom) at 300 m depth (left) and 900 m depth (right) in $m^2\,s^{-1}$ ($\log_{10}$ color scale). The respective first guess values are 10^3, 10^3 and 10^{-5} $m^2\,s^{-1}$. Each overlaid contour corresponds to a percentile of the observed stratification map $\frac{\partial \rho}{\partial z}(x,y)$ that is depicted at 300 m in Fig. 6 (bottom left). Black contours (resp. magenta contours) denote the 60th, 70th, 80th, 90th (resp. 10th, 20th, 30th, 40th) percentiles of $\frac{\partial \rho}{\partial z}(x,y)$.

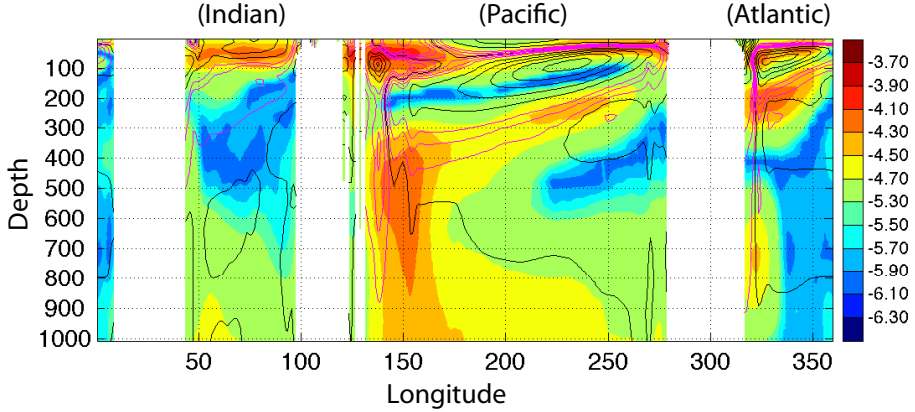

Figure 10. Estimated diapycnal diffusivity ($\mathcal{K}_d$) at the equator in $m^2\,s^{-1}$ ($\log_{10}$ color scale). Black and magenta contours denote the time mean zonal velocity from the state estimate. Black contours are separated by $10\,cm\,s^{-1}$ whereas magenta contours are separated by $4\,cm\,s^{-1}$ in the range within $\pm 10\,cm\,s^{-1}$.

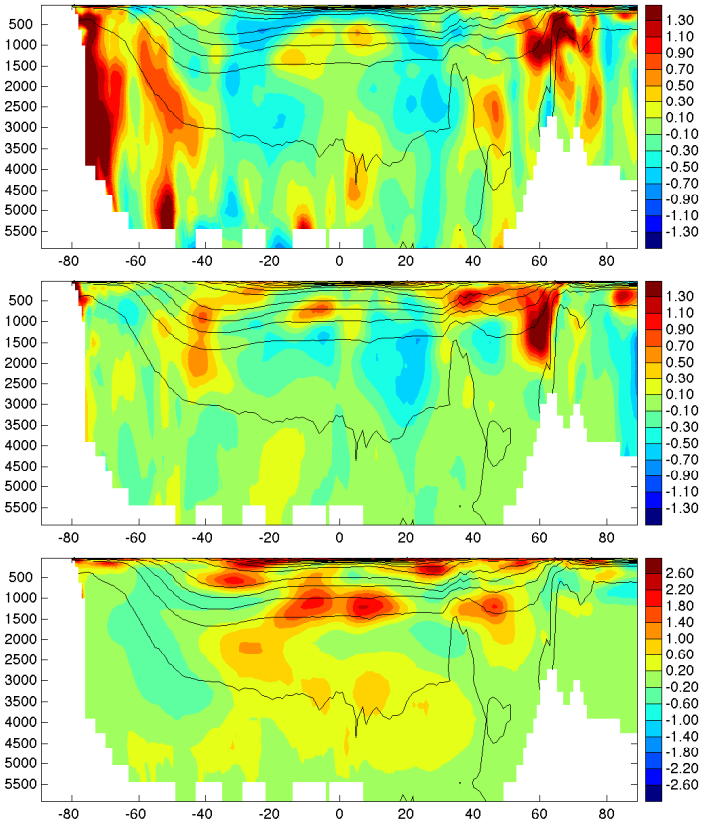

Figure 11. Zonal mean of $\frac{\mathcal{K}_{\mathrm{gm}}-K_{\mathrm{gm}}}{K_{\mathrm{gm}}}$ (top), $\frac{\mathcal{K}_{\sigma}-K_{\sigma}}{K_{\sigma}}$ (middle), and $\frac{\mathcal{K}_{\mathrm{d}}-K_{\mathrm{d}}}{K_{\mathrm{d}}}$ (bottom) with $K_{\mathrm{gm}} = 10^3$, $K_{\sigma} = 10^3$ and $K_{\mathrm{d}} = 10^{-5}\,\mathrm{m^2\,s^{-1}}$. Overlaid contours: zonal mean potential density from the OCCA atlas.

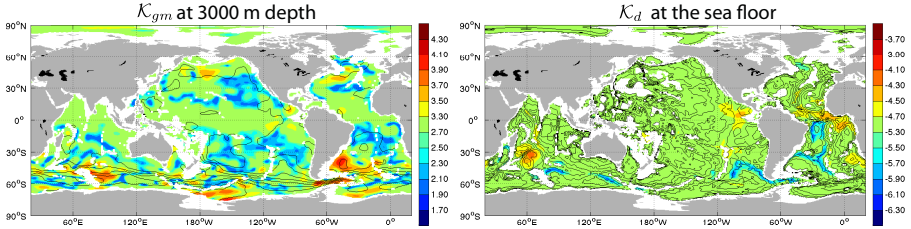

Figure 12. Estimated bolus velocity coefficient at 3000 m depth (left) and diapycnal diffusivity immediately above the sea floor (right) in $m^2\,s^{-1}$ ($\log_{10}$ color scale). Overlaid contours: σ_1 potential density from the OCCA atlas in 0.02 $kg\,m^{-3}$ increments (left) and ocean depth in 500 m increments (right).